



On the lightweight design of laminated insulating glass units in cruise ships

Downloaded from: <https://research.chalmers.se>, 2025-12-25 04:46 UTC

Citation for the original published paper (version of record):

Heiskari, J., Romanoff, J., Laakso, A. et al (2025). On the lightweight design of laminated insulating glass units in cruise ships. *Ships and Offshore Structures*, 20(12): 2035-2053.
<http://dx.doi.org/10.1080/17445302.2024.2403163>

N.B. When citing this work, cite the original published paper.



On the lightweight design of laminated insulating glass units in cruise ships

Janne Heiskari, Jani Romanoff, Aleksi Laakso & Jonas W. Ringsberg

To cite this article: Janne Heiskari, Jani Romanoff, Aleksi Laakso & Jonas W. Ringsberg (2025) On the lightweight design of laminated insulating glass units in cruise ships, *Ships and Offshore Structures*, 20:12, 2035-2053, DOI: [10.1080/17445302.2024.2403163](https://doi.org/10.1080/17445302.2024.2403163)

To link to this article: <https://doi.org/10.1080/17445302.2024.2403163>



© 2024 The Author(s). Published by Informa UK Limited, trading as Taylor & Francis Group



Published online: 13 Sep 2024.



Submit your article to this journal [↗](#)



Article views: 825



View related articles [↗](#)



View Crossmark data [↗](#)



Citing articles: 1 View citing articles [↗](#)

On the lightweight design of laminated insulating glass units in cruise ships

Janne Heiskari ^a, Jani Romanoff^a, Aleksi Laakso^b and Jonas W. Ringsberg^c

^aDepartment of Mechanical Engineering, Aalto University School of Engineering, Espoo, Finland; ^bMeyer Turku Oy, Turku, Finland; ^cDivision of Marine Technology, Department of Mechanics and Maritime Sciences, Chalmers University of Technology, Gothenburg, Sweden

ABSTRACT

Modern cruise ships employ many large windows to enable passengers to enjoy the marine environment. Most windows are insulating glass units (IGUs) consisting of laminated glass and a hermetically sealed cavity. These laminated IGUs exhibit three physical effects under bending: (1) geometric nonlinearity of the glass panes, (2) shear transfer in the laminated glass, and (3) load sharing due to the hermetically sealed cavity. The Authors have previously studied the (1) and (3) effects on the window mechanical behaviour and glass pane thickness determination. Hence, this paper investigates through optimisation how all these effects together lighten the IGUs, and how the shear transfer affects the IGU mechanical behaviour with the optimised thicknesses. All three combined effects have positive effects on the IGU weight. These results are more pronounced for large and thin IGUs subjected to high design loads. For example, the choice of interlayer material is less important (for optimum weight) for small windows subjected to a low design load. Since all the effects are important, using the finite element method is recommended to achieve a lightweight window design.

ARTICLE HISTORY

Received 1 February 2024
Accepted 13 July 2024

KEYWORDS

Cruise ship design; insulating glass unit; laminated glass; load sharing; nonlinear finite element analysis; shear transfer

1. Introduction

Passenger ships are complex floating structures, and a lot of research has been done on optimising their structural weight (e.g. Romanoff et al. 2013; Andric et al. 2019; Raikunen et al. 2019; Andric et al. 2020). This is necessary because the size of the ships has increased significantly in recent decades (see Figure 1). Optimizations usually consider the steel parts of the hull and the superstructure, which is justified when the area of the windows is small. However, a typical state-of-the-art cruise ship today is covered in windows, as are the facades of buildings (Bostick 2009). The purpose of windows is to enable passengers to enjoy the surrounding ocean view. Cabins often have large individual windows or fully glazed walls. Glass walls may also cover multiple deck heights in common areas (*c* in Figure 2), and dome-shaped glass structures (*a* and *b* in Figure 2) and smaller glass ceilings are a growing trend. However, this increased use of windows negatively affects the ship's weight and centre of gravity. It is, therefore, important to consider these windows appropriately in the ship's design.

1.1. Laminated IGU windows: class rules and standards

Insulating glass units (IGUs) that insulate the outdoor environment from indoor spaces are the focus of this research. IGUs are used, for example, in buildings, buses, ships, and trains. They consist of at least two glass panes separated by a hermetically sealed gas-filled cavity (see *c*, *d*, and *e* in Figure 3). The cavity provides thermal insulation, which is very important energy-wise to the ship and comfort-wise to the passengers. Thus, except for windscreens, all the glazing covering the ship's surface are IGUs. Most IGUs are designed to withstand wind loads on the upper decks and water pressure on the lower decks. Window failure prediction has been studied (Gerlach and Fricke 2016) as accidental failures have been

reported on some cruise ships (e.g. NSIA n.d.). Windows can also be accidentally hit by passengers or loose objects and must be designed and built to ensure safety.

Window design in ships must, therefore, always fulfill the rules set by the classification societies. The following societies are considered here: Det Norske Veritas (DNV 2022), Bureau Veritas (BV 2022), and Lloyd's Register (LR 2022). These specify how the monolithic glass pane thickness (*a* in Figure 3) and glass pane thickness in laminated glass (*b* in Figure 3) are calculated, what is the minimum allowed glass thickness, what types of glass panes are allowed, and what are the design loads. The required minimum monolithic glass pane thickness is calculated based on the linear plate theory so that the maximum principal stress does not exceed the 40 MPa limit. However, it is well known that as the deflection of thin-walled plates grows large, the von Kármán strains (i.e. geometric nonlinearities) make the structure stiffer (see Figure 4). This has a significant beneficial effect on the deflection and stresses of glass panes (Heiskari et al. 2022a) and is further promoted because all the glass panes in ships must be fully tempered (chemical strengthening is allowed in some cases), which itself increases the bending strength of the glass panes. The ISO 11336-1 standard (ISO 2012) for ships gives a characteristic failure strength of 160 MPa for fully tempered glass. The design strength is obtained from this with a safety factor of four. These treatments also reduce the shard fragment size in case of glass failure, which is important for safety. For example, the EN 12150-1 standard (SFS-EN 2015) defines that for a fully tempered glass pane with thickness between 4 and 12 mm, there must be at least 40 shards in a 50 mm times 50 mm area.

Further safety is achieved by using laminated glass (*b* in Figure 3). The IGUs on cruise ships typically have either one laminated glass and one monolithic glass (*d* in Figure 3), or two laminate (*e* in Figure 3) depending on the window's location. The laminated glass consists of at least two monolithic glass panes glued together by a polymeric

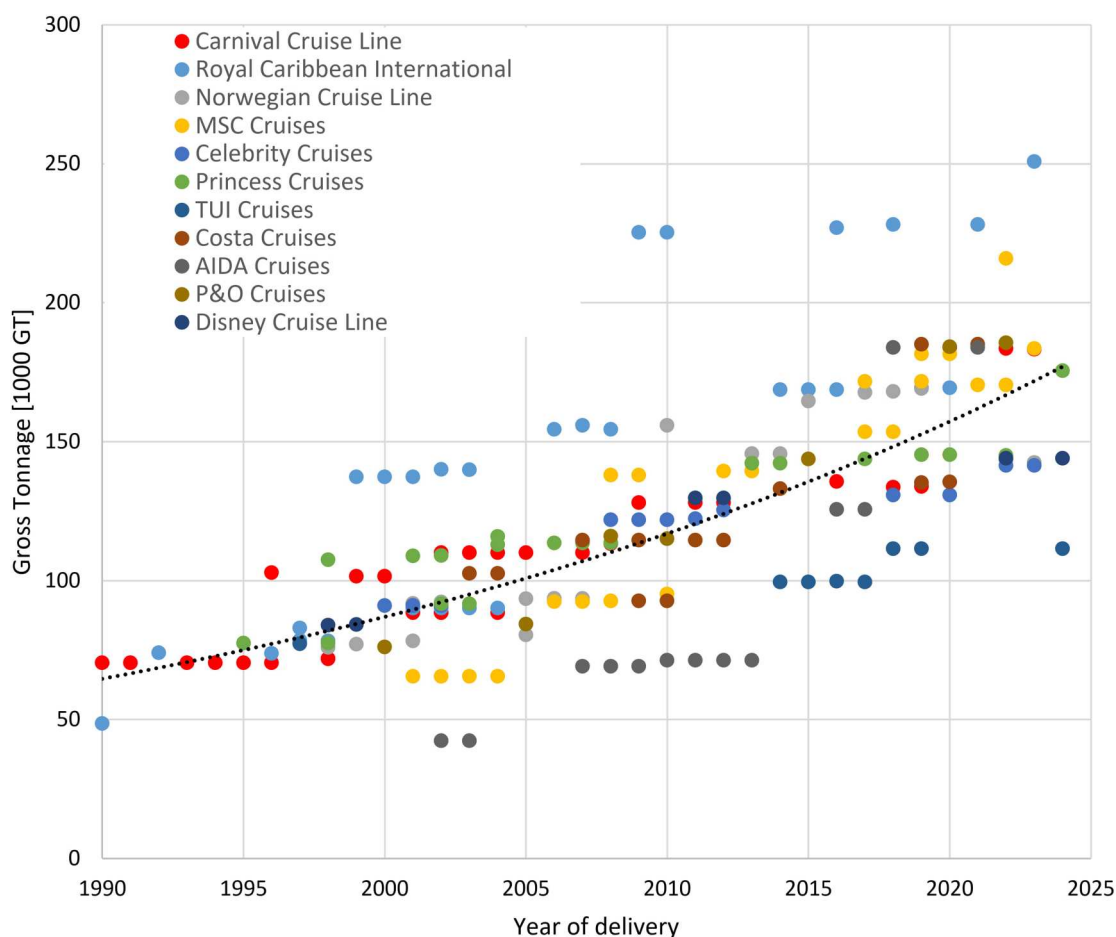


Figure 1. The development of cruise ship size. (This figure is available in colour online.)

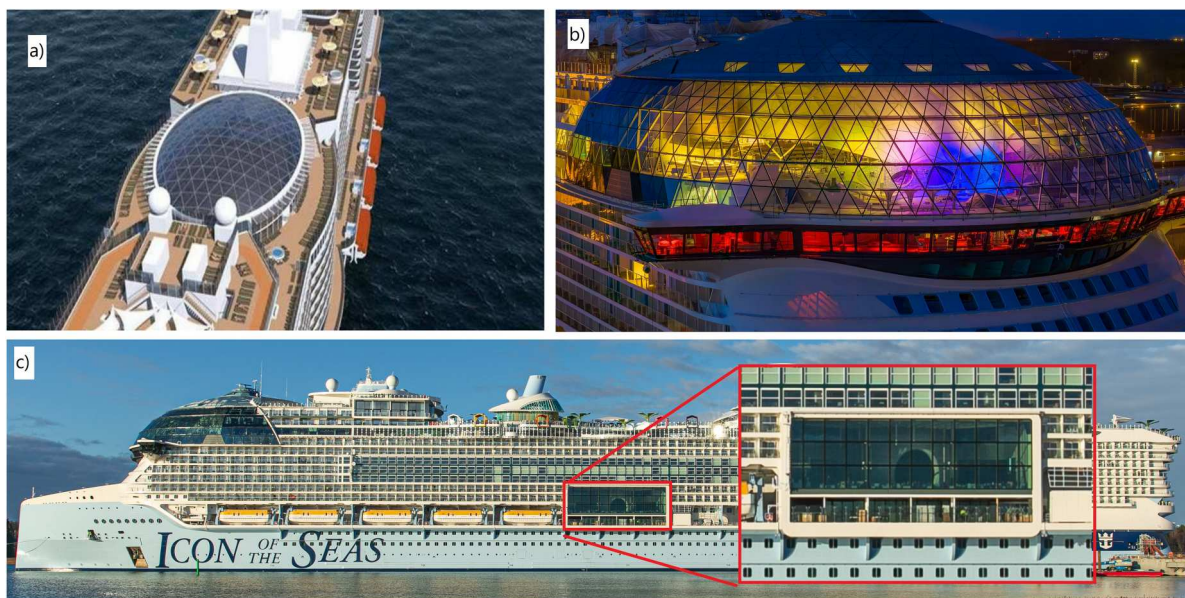


Figure 2. Examples of ship windows: (a) SkyDome from M/S Iona (2018) (courtesy of Francis Design), (b) AquaDome from Icon of the Seas (2023) (photo credit Niko Alakoski), and (c) side view of Icon of the Seas showing a large glass wall (photo credit Tuukka Salo /Mediascope productions). (This figure is available in colour online.)

interlayer. Its purpose is to retain broken shards and prevent them from falling on passengers if the windows break. The two most common interlayer materials in ship windows are polyvinyl butyral

(PVB) and ionomer (SentryGlas Plus®(SGP) from Kuraray America, Inc.). The latter is more expensive but is significantly stiffer than the former.¹ This is important because the polymeric interlayers are

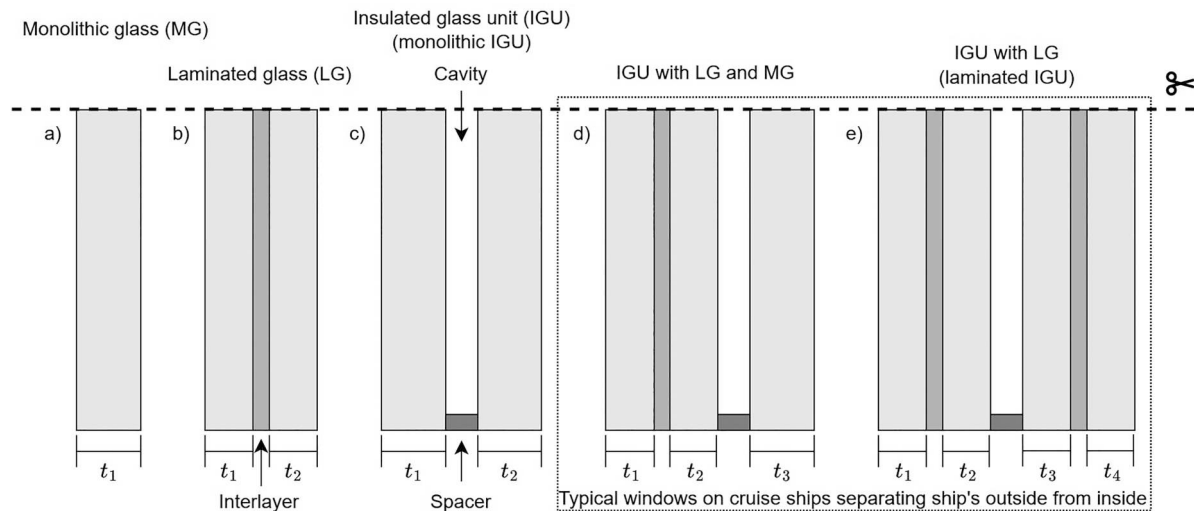


Figure 3. Different types of windows with glass pane thicknesses.

viscoelastic, meaning the stiffness properties depend on temperature and loading time. The longer the loading time and the higher the temperature, the less stiff the interlayer is. The stiffness then determines how well the loads are transferred between the glued glass panes; this is the shear transfer (Figure 4). Including shear transfer in the laminated glass structural design has gained importance (Kuntsche et al. 2019) and is included in the classification rules (see Appendices A.1, A.2 and A.3). Because ship windows are exposed to hot weather and direct sunlight, choosing a stiffer interlayer is tempting, as it is structurally a better option. However, it could lead to unnecessarily high-load-bearing laminated glass panes, which is not cost-effective for cruise ships.

Looking at the IGU structure, the sealed cavity in the IGU allows for a load sharing effect (see Figure 4) to occur between the glass panes. This increases the window's load-bearing capacity and reduces the deflections and stresses (Heiskari et al. 2022a). The load sharing has been the subject of several studies (e.g. Vallabhan and Chou 1986; Wörner et al. 1993; McMahon et al. 2018; Galuppi and Royer-Car-fagni 2020; Respondek et al. 2022). Note that the load sharing effect is different from the shear transfer effect. The former occurs in IGUs and the latter in laminated glass. While the shear transfer is considered in the class rules, load sharing and geometric nonlinearity are not considered. Neglecting these two effects may result in up to 50% thicker glass panes than necessary (Heiskari et al. 2022a, 2023), which is not weight-effective for cruise ships.

1.2. Objective of study

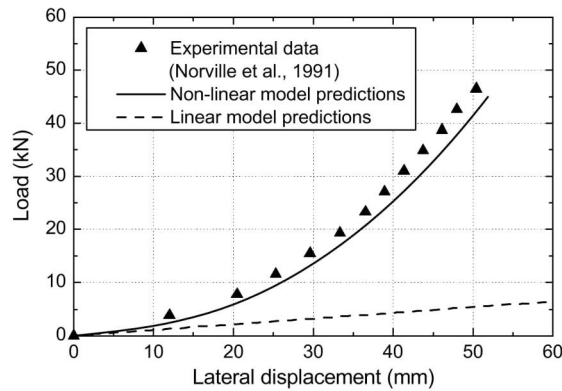
The increased use of windows on ships means that there are a lot of large cut-outs in the hull on the ships' sides. Their effect on a ship's global response has been studied by Fricke and Gerlach (2015). However, there is a lack of study on the glass weight problem that considers the actual window structure sufficiently. Laminated glass has been optimised to reduce weight and cost by using the maximum principal stress and the deflection criteria (Foraboschi 2014), but the analysis method was based on linear plate theory and did not include the IGU construction, i.e. the load sharing. On the other hand, load sharing and geometric nonlinearity have been studied for the thickness determination of monolithic IGUs (c in Figure 3) (Heiskari et al. 2022a, 2023). That is, no shear transfer was considered. Therefore, the goal of this study is to optimise the laminated IGU type of windows considering all three effects to

find the smallest glass pane thicknesses by using methods and knowledge available in the ship's concept design phase. This typically means that the analyst knows the size and shape of the window, the configuration (Figure 3), the material properties (interlayer), and the design load. Furthermore, the thickness calculation must be fast and accurate to estimate weight. For brevity, only rectangular laminated IGUs of three different sizes are considered – (1) $a = b = 1500$ mm, (2) $a = 2500$ mm $b = 1500$ mm, and (3) $a = b = 3500$ mm (a is the longer side). Two different uniformly distributed design loads are applied in a quasi-static manner – (1) 2.5 kPa, and (2) 15.0 kPa. Two different interlayer materials are used with three different stiffness properties due to temperature change² – (1) PVB, and (2) SPG at (i) 25°C, (ii) 35°C, and (iii) 50°C. Hence, the total number of optimised cases is 36. The nonlinear finite element method is combined with the Particle Swarm Optimization (PSO) (Kennedy and Eberhart 1995) routine to obtain the response. These include maximum deflection and maximum principal stress of the glass panes, which are both used as design criteria. The results are expected to demonstrate how shear transfer affects the laminated IGU mechanical behaviour under large deflections with optimised glass pane thicknesses combined with the geometric nonlinearities and load sharing, how much weight can be saved with respect to the current classification rule methods, and whether choosing the stiffer but more expensive interlayer is justifiable (from a structural weight point of view). Hence, this paper aims to enhance the accuracy and understanding of window thickness calculation in a ship's concept design phase, which is important for exploring the feasibility of different design variants.

2. Complexity and challenges in laminated glass design

When the laminated glass bends, the stresses are transferred through the interlayer between the glass panes. The shear transfer can be divided into three categories: (1) no shear transfer, (2) partial shear transfer, and (3) full shear transfer (as shown in Figure 4). (1) and (3) can be called the layered and monolithic limits, respectively. The glass panes bend independently without the shear transfer, and the interlayer is completely neglected. That is, there is a linear stress distribution in *each glass pane* through the thickness. In the monolithic limit, the interlayer is considered fully active, and there is a linear stress distribution through the *whole laminated glass*

Geometric nonlinearity



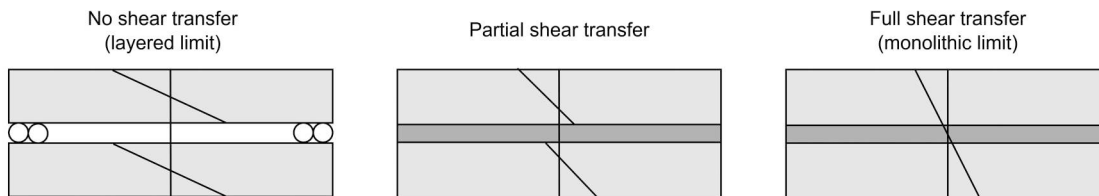
The von Kármán strains through the thickness

$$\varepsilon_{bending} + \varepsilon_{membrane, vK} = \varepsilon_t$$



Shear transfer

Normal stress distribution through the thickness



Load sharing

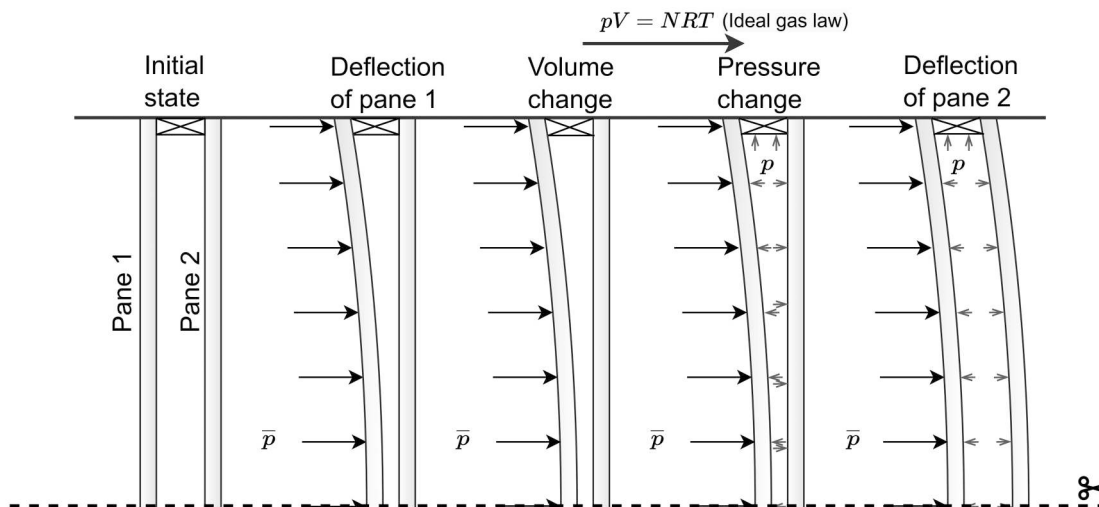


Figure 4. A summary of the mechanical effects occurring under the bending of windows. Geometric nonlinearity: comparison between linear and nonlinear predictions for a glass pane (Haldimann et al. 2008) and the role of von Kármán strains on the overall stress state through the thickness (bending + membrane = total). Shear transfer: through-thickness normal stress distribution for varying degrees of shear transfer in laminated glass. Load sharing: (1) two glass panes in an IGU are in the initial state, (2) an external load is applied to the first glass pane resulting in deflection, (3) the deflection reduces the cavity volume, (4) the cavity volume change results in increased cavity pressure according to the ideal gas law, and (5) the second glass pane will deflect under the cavity pressure (Heiskari et al. 2022a). The cavity pressure is p , V is the cavity volume, N and R are the cavity gas properties, and T is the cavity temperature.

thickness. With partial shear transfer, there is a *zigzag* stress distribution through the whole thickness. Laminated glass panes are practically always in this partial mode. However, the behaviour approaches the monolithic limit with very stiff SGP interlayers. Similarly, the behaviour approaches the layered limit with more flexible interlayers.

There are different methods of analysing the behaviour of laminated glass panes, including shear transfer. A practical approach is to use something called the *effective thickness* (e.g. Galuppi and Royer-Carfagni 2012b, 2012a). A single effective thickness derived for stress or stiffness-based equivalency replaces the layered structure with multiple thicknesses. The degree of shear transfer is

then included in this effective thickness. However, this method requires different thicknesses for the response: one for the deflection and another for the stresses, which makes the method unsuitable for structural optimisation with multiple constraints. Additionally, this method may require a shape parameter, which is dependent on the window shape and size, and boundary conditions (see Appendix A.4). Other effective thickness approaches can be found in some standards (e.g. EN 16612 SFS-EN 2019). An analytical solution for a simply-supported laminated glass was formulated by Foraboschi (2012). This yields an exact solution but works only for the linear region and is limited by the boundary conditions. To overcome these, the response can be obtained using the finite element method (FEM) with a laminated shell element developed by Liang et al. (2016). This element models the zigzag behaviour and includes the viscoelasticity of the interlayer material. However, such an element is not readily available in commercial FE packages. An alternative method is exploited here; the laminated glass is modelled using solid-shell elements (continuum shells) that possess a continuum solid topology. Fröling and Persson (2013) have used this type of analysis and obtained accurate results with respect to the displacements and stresses. Another solid-shell element study was conducted by Magisano et al. (2023), who included the nonlinear response with good results. Since it is necessary to get an accurate response of laminated IGUs of various shapes, sizes, and thickness configurations, nonlinear FEM with solid-shell elements for the laminated glass is chosen as the analysis method in this paper.

3. Structural analysis: finite element model of laminated IGU

The finite element model of the laminated insulated glass unit is described in the ANSYS Mechanical APDL. First, the used elements are explained. Then, a mesh convergence study is conducted to find the proper element size, and the behaviour of the solid-shell element is studied more closely with the resulting element size. Finally, the model is validated with the experimental results of McMahon et al. (2018).

3.1. Elements

The different element types are explained first (see Figure 5 for a graphical explanation). The glass panes and the interlayer are modelled with 8-node solid-shell elements (SOLSH190 in ANSYS ANSYS 2024c). They are used to model thin to moderately thick shell structures. The element has a 3D topology and eight nodes with three translation degrees of freedom in each node. The

advantage of the solid-shell element over the single-layer shell element is that it has two nodes thickness-wise, which allows for modelling the shear transfer in a laminated glass more accurately (zigzag). Thus, there is no need to use separate thickness scaling based on deflection or stress (effective thickness method). The advantage over the solid element is that the solid-shell element is less prone to shear locking in bending dominant problems (ANSYS 2024c). Hence, it is sufficient to use only one solid-shell element through the thickness of each layer. The cavity volume is modelled with a 5-node hydrostatic fluid element (HSFLD242 in ANSYS ANSYS 2024a) that follows the ideal gas law. This element has three translation degrees of freedom in the 'base' nodes (I, J, K, L in Figure 5) and a pressure degree of freedom in the apex node (Q in Figure 5). The hydrostatic fluid elements are placed on top of the structural elements that face the cavity. The spacers are modelled with 4-node shell elements (SHELL181 in ANSYS ANSYS 2024b) that have six degrees of freedom in each node – three translations and three rotations. Their purpose is solely to create the enclosed cavity and not to participate structurally (modeled with low stiffness and thickness as done by Heiskari et al. 2022a, 2023).

3.2. Boundary conditions

The windows cannot be bonded so tightly that fixing all edge translations is realistic when large deformations are considered. Such boundary conditions are often used in the standards/rules because they are based on linear assumptions (i.e. small deformations). At large deflections, the validation by Heiskari et al. (2022a) showed that such boundary conditions heavily underestimate the deflections; therefore, a boundary condition allowing for sliding of the edges is used. An additional set of shell elements (4-node SHELL181) are added to the top and bottom edges of the solid-shell elements representing the supports, such as silicone sealant bonding (see Figure 6). It should be noted that the windows are typically bonded only on one side; this is just a modelling trick to avoid giving the spacers the real stiffness properties, which may not be such a trivial task. The geometric boundary conditions are applied to the 'free' edges of these support elements. An alternative way of giving the same boundary conditions is shown in Figure 8 where no support elements are used. The out-of-plane translation constraints are simply placed on the edges of the laminated glass, and rigid body motion must be prevented by constraining some of the middle nodes in the in-plane direction. This becomes very difficult for irregular triangular shapes, which cruise ship windows often have. Therefore, the first modelling method is preferred.

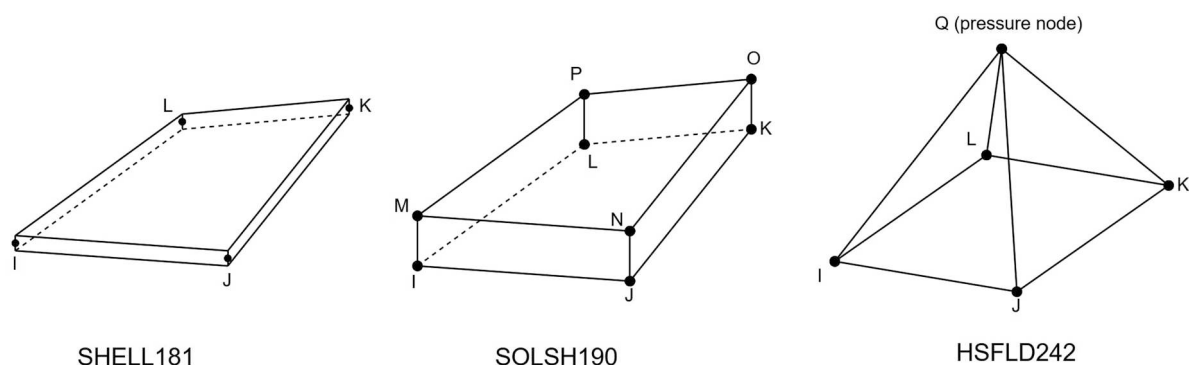


Figure 5. The used elements in Ansys: 4-node structural shell element (ANSYS 2024b), 8-node solid-shell element (ANSYS 2024c), and 5-node hydrostatic fluid element (ANSYS 2024a), respectively.

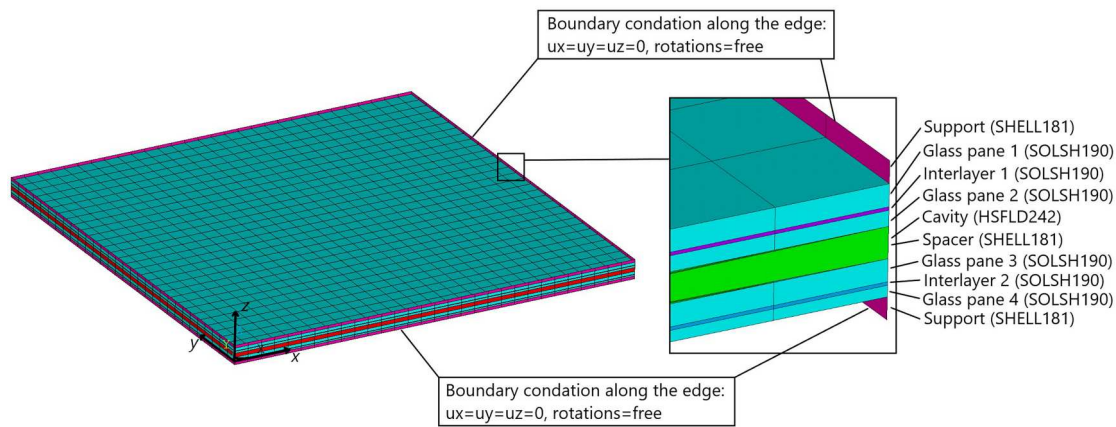


Figure 6. A 1500×1500 meshed rectangular laminated IGU with an element size of 50 mm. The magnified edge cut section shows the through-thickness composition with the corresponding element types. The spacer elements are not visible because they are behind the cavity elements. The boundary conditions are applied around the whole perimeter of the support edges. The uniformly distributed load is applied on the surface of glass pane 1 in the direction of $-z$. Note that the glass panes can slide in the in-plane direction with the x -, y -, and z -translation restraints on the support. (This figure is available in colour online.)

3.3. Analysis model

Figure 6 illustrates the meshed analysis model with its different components and corresponding element types. The element colours represent different materials, but both interlayer materials have identical properties in this study. All the analyses are conducted on a nonlinear basis (i.e. NLGEOM, on) with the Newton-Raphson method and the load is quasi-static. Note that the nonlinear analysis only includes geometric nonlinearities. The interlayers are modelled as linear elastic materials. The viscoelasticity is only considered by changing Young's modulus based on the manufacturer's tables (e.g. Kuraray 2024) for different loading times and temperatures (as is the practical engineer approach).

3.4. Mesh convergence and element aspect ratio analysis

The objective here is to find the minimum element size that is practical for the engineering optimisation problem. Therefore, the stresses and deflections must be accurate enough, and the computational time must be reasonable. Therefore, the hexahedron element size is increased from 30 mm to 100 mm in increments of 10 mm to study the element size effect on the deflection and the maximum principal stress of the glass panes. The load and the pane thickness are chosen as 15 kPa (a typical load for windows closer to sea level) and 10 mm, respectively, for producing stresses at the same magnitude as the design strength in the classification rules (40 MPa). The interlayer's Young's modulus is chosen as 1.8 MPa, which corresponds to PVB interlayer at 1 minute loading time and 25°C (see Table 2). Three rectangular IGU sizes are used: (1) $a = b = 1500$ mm, (2) $a = 2500$, $b = 1500$ mm, and (3) $a = b = 3500$ mm (a is the longer side and b is the shorter side). The results are shown in Figure 7. The deflection changes 3.4% at maximum when the element size is increased from 30 mm to 100 mm. This corresponds to 0.2 mm in absolute value. Hence, the element size does not significantly influence the deflection. However, the stress change for the largest IGU is 6% when the element size is increased from 30 mm to 100 mm. The change is only up to 3% with the element size of 50 mm. This is chosen as it is notably less computationally heavy than the 30 mm element size, and the errors are at a reasonable range. The resulting number of elements, nodes, and degrees-of-freedom for the different IGU sizes are shown in Table 1. The selected mesh gives an aspect ratio for the thinnest solid-shell elements of $50/1.52 \approx 33$. Ansys does have a limit for the ratio, but a user

can specify it. Ansys gives a shape warning (which does not interrupt the simulation or automatically make the results invalid) after it is reached. No such limit is used in this study, and therefore, the aspect ratio is studied next more closely.

To ensure that such thin solid-shell elements still work well for bending problems, a smaller laminated glass model is studied where it is possible to reduce the element size more than in the actual laminated IGU model. A laminated glass with side lengths of $a = 600$ mm and $b = 200$ mm is chosen with pane thicknesses of 4 mm and interlayer thickness of 1.5 mm. The interlayer Young's modulus is 1.8 MPa. The model is constrained vertically (z -direction) on two opposing sides to allow for sliding in the in-plane direction. The model is further constrained at the centre of the plate in the x - and y -direction to prevent rigid body motion. The meshed model is shown in Figure 8. A uniformly distributed load of 8.0 kPa, chosen to produce a relatively large deflection, is applied to the surface for nonlinear analysis. Seven element sizes are used: 4, 5, 10, 20, 25, 50, and 100 mm, yielding aspect ratios of 2.7, 3.3, 6.7, 13.3, 16.7, 33.3, and 66.7 for the interlayer element, respectively. The response is obtained in the centre of the laminated glass bottom surface ($(x, y, z) = (300, 100, 0)$). The deflection and stresses are shown in Figure 9. The deflection is 11.0 mm for the smallest element size and 10.6 mm for the largest. On the other hand, the deflection difference is 0.1 mm between the smallest element size and 50 mm element size (which is used in the large IGU model). This is an error of $\approx 1\%$. For the stresses, the difference between the smallest element size and the 50 mm element size is 1.8 MPa and 0.4 MPa in the x - and y -direction, respectively. These correspond to errors of 3.6% and 3.4%, respectively. The numerical error increases with the element size and aspect ratio of the elements but is still at acceptable levels. The errors are less significant for the actual IGU models at large deflections because the membrane action becomes more dominant (von Kármán strains). Besides, some accuracy must be sacrificed when structures are optimised in a ship's concept design phase.

3.5. Validation

This subsection aims to ensure that the presented laminated IGU model can accurately predict the deflections so it may be used in the later sections to optimise the glass pane thicknesses. The laminated glass panes are treated as monolithic by ascribing the glass material properties to the interlayer for validation. That is, the model is a simple IGU with both monolithic panes having three 3D solid-shell elements

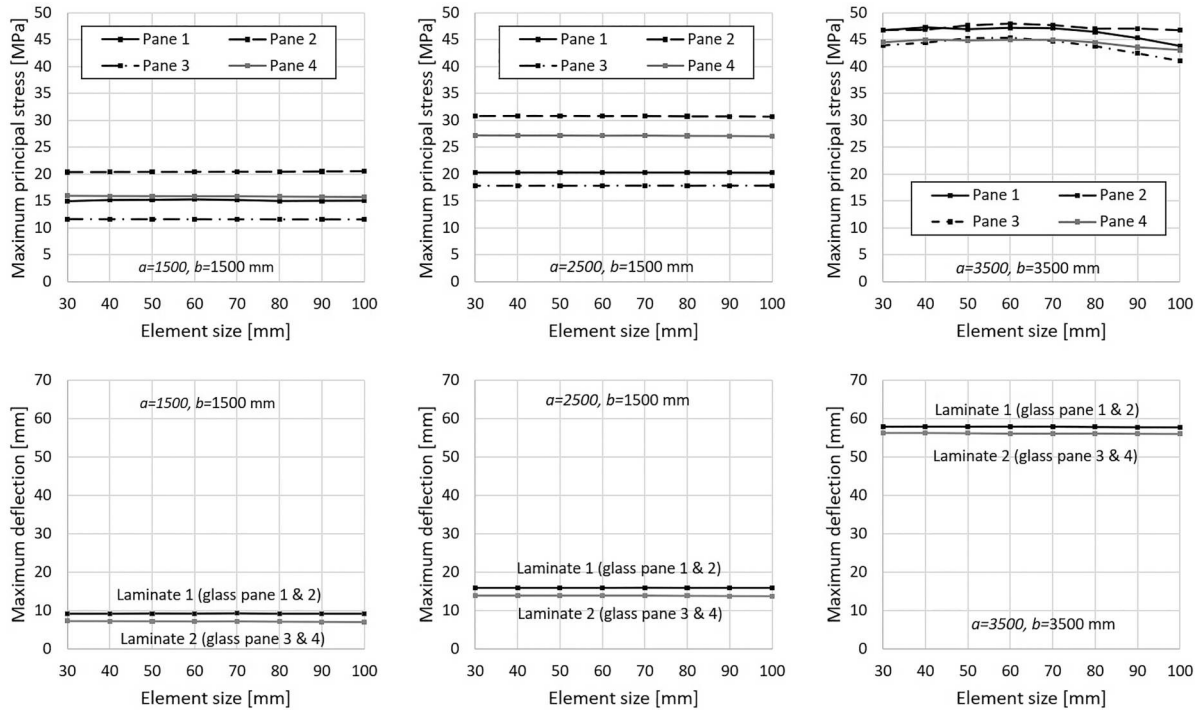


Figure 7. Mesh convergence analysis of rectangular laminated IGUs of three sizes. The applied load is 15 kPa, and the boundary conditions are shown in Figure 6. The top row presents the maximum principal stresses of each glass pane of each IGU size, while the bottom row presents the maximum deflections.

Table 1. Number of elements, nodes, and degrees of freedom (DOFs) for each meshed laminated IGU model.

Size	No. of elements	No. of nodes	No. of DOFs
1500 × 1500	8348	7928	25,228
2500 × 1500	13,828	12,968	40,828
3500 × 3500	44,668	40,888	126,028

through the thickness. This is because no published experimental results are available for laminated IGUs under bending (at least to our knowledge). The results have been compared with experimental results by McMahon et al. (2018) and with numerical results by Heiskari et al. (2022a), where the monolithic IGU FE model is presented with 2D shell elements. For this reason, the size of the rectangular IGU is chosen as $a = 1260$ mm, $b = 750$ mm, $s = 13$ mm, and $t_1 + t_2 + t_{int} = t_3 + t_4 + t_{int} = 5.7$ mm. The uniformly distributed load varies from 0 kPa to 7 kPa in increments of 0.5 kPa. For the FE model, the supports are given the following material properties: $E = 500$ MPa, $\nu = 0.3$, and thickness $t_s = 1$ mm. The analysis considers geometric nonlinearities. The results are shown in Figure 10 and are close to the experimental results with relative errors of 7.7 % and 5.6 % for panes 1 and 2, respectively, for the largest load. Further, the 3D solid-shell FE results are almost identical to those obtained by Heiskari et al. (2022a) for the IGU model with the 2D shell elements. That model was also validated against analytical methods on a linear basis. Therefore, it can be concluded that the model with the additional support elements for applying the geometric boundary conditions is working correctly. This also further demonstrates that the model behaves well under bending, even when the thinnest elements have an aspect ratio of 33.

4. Particle swarm optimisation

Particle swarm optimisation (PSO) (Kennedy and Eberhart 1995) is a metaheuristic optimisation algorithm that has proven to be

powerful, e.g. in optimising ship structures (Raikunen et al. 2019; Romanoff 2014). One of its strengths is that it does not require gradient information – only design variables, the objective function(s), and equality and/or inequality constraints are enough. PSO is stochastic and uses a ‘trial and error’ type of search process. In the current study, this means that the four different glass pane thicknesses (e in Figure 3) are randomly generated in MATLAB at the beginning of the PSO routine, and MATLAB creates the corresponding input file for Ansys. Then MATLAB calls and executes the Ansys simulation, which solves the response. The MATLAB algorithm then checks the feasibility of the current design (thickness values). Based on this information, the PSO algorithm calculates new thicknesses in MATLAB, and the process is repeated until the function gives the optimum solution. That is, the thicknesses that produce the least weight without breaking the design constraints. The optimisation flowchart is shown in Figure 11.³

The PSO has a swarm that consists of a certain number of particles. These are denoted with an index i . Each particle has a position vector $\vec{x}_i(t)$ and a velocity vector $\vec{v}_i(t)$. The former is the particle’s current position, and the latter shows the direction in which the particle moves. Both are updated at each iteration t . At all times, each particle remembers its personal best position $\vec{P}_i(t)$, and all particles know the global best position $G(t)$. Once the first iteration is completed with the initial positions, a new position is calculated as:

$$\vec{x}_i(t+1) = \vec{x}_i(t) + \vec{v}_i(t+1). \quad (1)$$

The velocity vector may be calculated using the current velocity (initially 0), the personal and the global positions, and certain coefficients:

$$\vec{v}_i(t+1) = w\vec{v}_i(t) + r_1c_1[\vec{P}_i(t) - \vec{x}_i(t)] + r_2c_2[G(t) - \vec{x}_i(t)] \quad (2)$$

where r_1 and r_2 are random numbers with intervals of 0 and 1. The movements of the particles are visualised in Figure 11. The

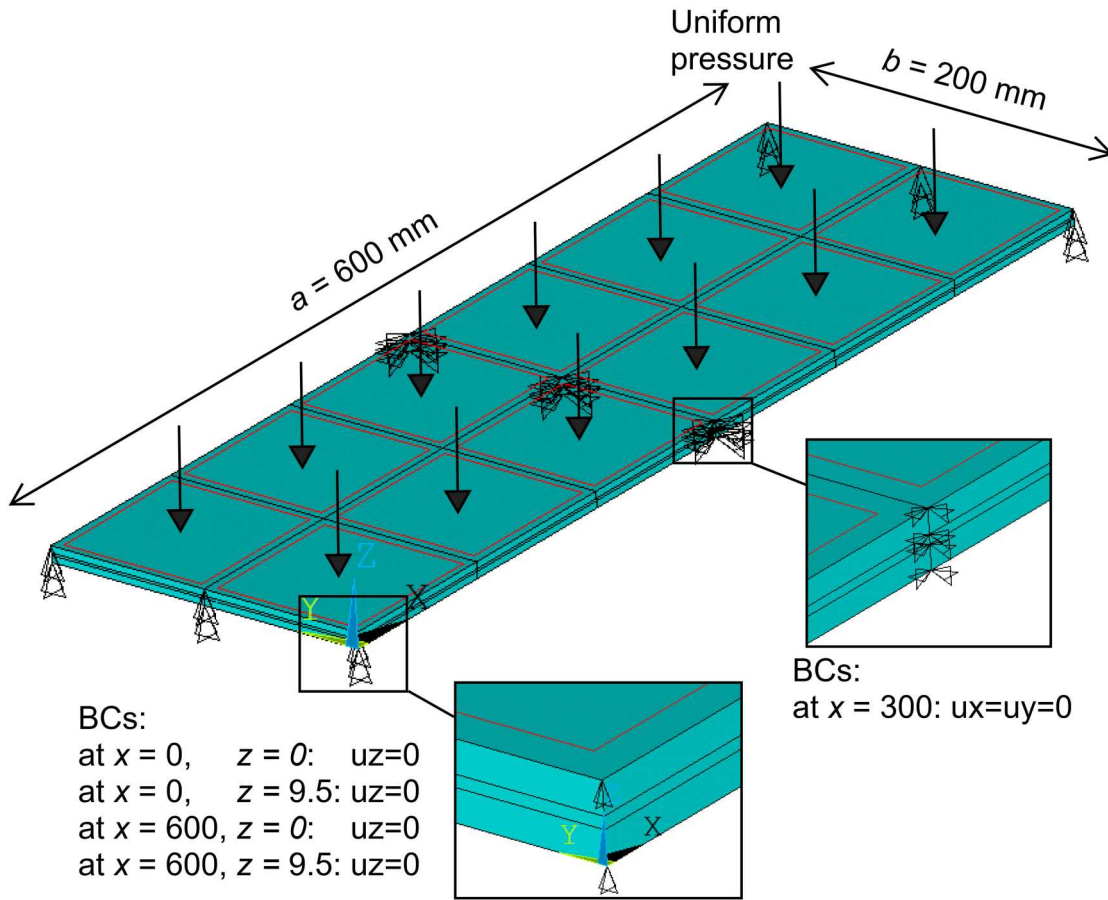


Figure 8. Meshed model of a $600 \times 300 \text{ mm}$ laminated glass with a glass pane thickness of 4 mm and interlayer thickness of 1.5 mm . This model is used to study the effect of the solid-shell aspect ratio on the deflections and stresses. The load is uniformly distributed on the top surface with a magnitude of 8 kPa . The boundary conditions are shown in the figure. The analysis type is nonlinear static structural. Note that the element size in this figure is the largest (100 mm). The response is obtained in the middle of the bottom surface ($x = 300, y = 100, z = 0$). (This figure is available in colour online.)

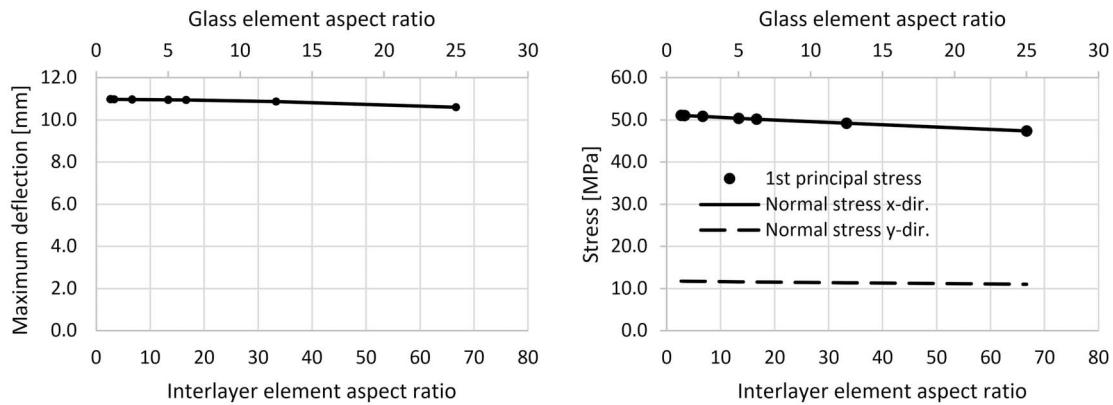


Figure 9. Deflection and the stresses in the middle of the bottom surface ($x = 300, y = 100, z = 0$) of the laminated glass model in Figure 8.

coefficients c_1 and c_2 are calculated as:

$$\begin{aligned} c_1 &= \chi \phi_1 \\ c_2 &= \chi \phi_2 \\ w &= \chi \\ \chi &= \frac{2\kappa}{|2 - \phi - \sqrt{\phi^2 - 4\phi}|} \\ \phi &= \phi_1 + \phi_2 \end{aligned} \quad (3)$$

where $\kappa = 1$, $\phi_1 = 2.05$, and $\phi_2 = 2.05$ (Clerc and Kennedy 2002). Here, no further damping is used. The c coefficients are acceleration

coefficients, and w is the inertia coefficient. The velocities are limited by using the range that a particle can take values of:

$$\begin{aligned} \text{Velocity}_{ij, \max} &= \frac{\text{Variable}_{ij, \max} - \text{Variable}_{ij, \min}}{f} \\ \text{Velocity}_{ij, \min} &= -\text{Velocity}_{ij, \max} \end{aligned} \quad (4)$$

where $f = 5$, which the Authors have found to be sufficient by trial and error process. The index j describes the variable number that each particle has. The Equations (3) and (4) are used to ensure that the particles do not take too large steps and potentially

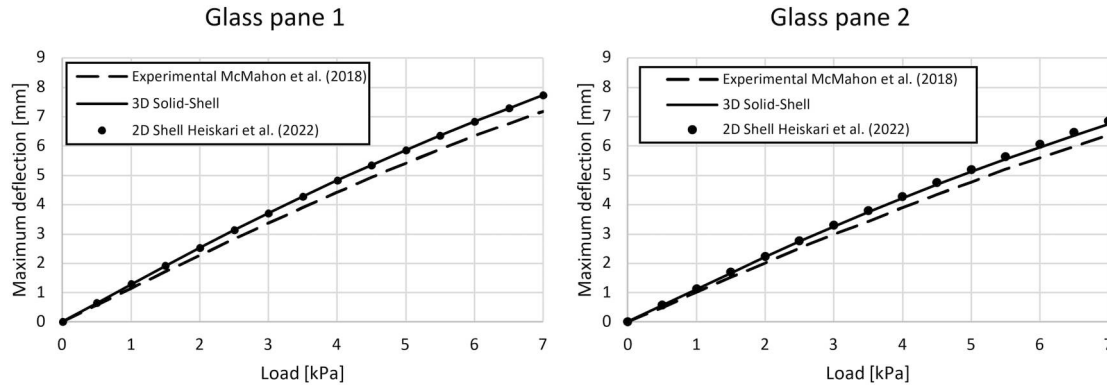


Figure 10. Comparison of 1260 × 750 mm monolithic IGU with glass pane thicknesses of 5.7 mm and cavity thickness of 13 mm: experimental results by McMahon et al. (2018), nonlinear FE analysis with 2D shell elements (Heiskari et al. 2022a), and nonlinear FE analysis with 3D solid-shell elements. Pane 1 is the directly loaded glass pane, and pane 2 is loaded through the load sharing effect.

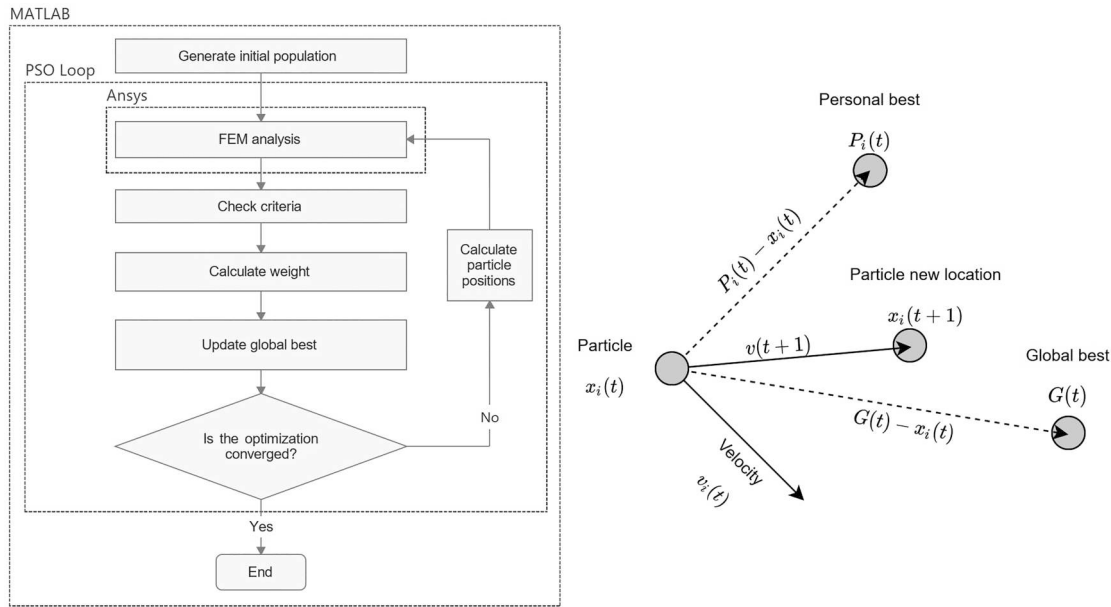


Figure 11. Flowchart of the optimisation routine and determination of the new particle position in PSO.

skip over the optimum solution. There are studies on how to improve the performance of the PSO routine (e.g. He et al. 2019; Freitas et al. 2020), but the presented and used ‘basic’ routine is sufficient for the current optimisation problem as it converges to the optimum solution with reasonable computational efforts.

4.1. Optimization problem

This study has four design variables, meaning that $j=4$ and the optimisation is four-dimensional. That is, each particle contains information for four variables. The objective function that the PSO tries to minimise is:

$$\text{Minimize } M(t) = \sum_{j=1}^4 t_j A \quad (5)$$

where M is the IGU weight (consisting of only glass), t is the glass pane thickness, and A is the glass pane area. The design constraints

limit this objective function:

$$\begin{aligned} \sigma_+ &\leq \sigma_{+,d} \\ \delta &\leq \frac{b}{\delta_d} \\ 1/r &\leq t_1/t_2 \leq r \\ 1/r &\leq t_3/t_4 \leq r \\ t_1 + t_2 &\leq r(t_3 + t_4) \\ t_3 + t_4 &\leq t_1 + t_2 \\ t_{lower} &\leq t_{1,2,3,4} \leq t_{upper} \end{aligned} \quad (6)$$

where σ_+ is the maximum principal stress, δ is the deflection, b is the shorter side of the rectangular glass pane, subscript d is the design value, and r is the thickness ratio. Maximum in-plane translation is not used as a criterion because it is critical only for rectangular windows with very high aspect ratios a/b (Heiskari et al. 2022b, 2023). The maximum nodal stresses and deflections are obtained from each glass pane (see Figure 11 in (Heiskari et al. 2022a) for additional details) and they are compared with the

design values:

$$\eta_{c1} = \frac{\max[\max(\sigma_{+,1}), \max(\sigma_{+,2}), \max(\sigma_{+,3}), \max(\sigma_{+,4})]}{\sigma_{+,d}} - 1 \quad (7)$$

$$\eta_{c2} = \frac{\max[\max(\delta_1), \max(\delta_2), \max(\delta_3), \max(\delta_4)]}{\delta_d} - 1.$$

From these, the maximum is found:

$$\eta = \max[\eta_{c1}, \eta_{c2}]. \quad (8)$$

Depending on the η sign, the weight is calculated as:

$$M(t) = \begin{cases} \sum_{i=1}^4 t_i A, & \text{if } \eta \leq 0 \\ \sum_{i=1}^4 t_i A(1 + 100\eta), & \text{otherwise.} \end{cases} \quad (9)$$

That is, if η is negative, the candidate particle is a feasible solution. If η is positive, then the particle is unfeasible, and a penalty is added to the weight. The algorithm is stopped once the weight has not improved in four consecutive iterations.

5. Case study

5.1. Design parameters and constraints

The four glass pane thicknesses are the optimisation variables. Three different temperatures are considered in the optimisation that affect the interlayer material properties. The lowest temperature is 25°C and the loading time is 1 minute. This condition is what the classification societies typically require at *minimum*. The material properties for the chosen conditions are shown in Table 2. Three rectangular sizes are considered: (1) $a = b = 1500$ mm, (2) $a = 2500$ mm $b = 1500$ mm, and (3) $a = b = 3500$ mm. The first one represents a typical smaller square window, the second one is a larger window that can cover a full deck height, and the third is a very large window. The spacer thickness is 14 mm. The design loads are chosen as 2.5 kPa and 15 kPa, which are typical for windows in ships on the upper decks and on decks closer to sea level, respectively.

All the constraints are shown in Table 3. The lower limit for a single glass pane thickness is set as 4 mm. Only discrete thickness values are used in the Ansys simulation. The initial thickness values generated by MATLAB and the updated thickness values by Equation (1) are continuous but rounded off to the nearest discrete value in MATLAB. The maximum allowed deflection is given by $b/100$, and the maximum allowed principal stress is 40 MPa. The former is the same limit as used by Heiskari et al. (2023). The deflection limit may originate from the spacer manufacturers to ensure the sealing of the cavity. The thickness ratios of the glass panes (Equation 6) are controlled with parameter r , which is set to 2 as it was found by Heiskari et al. (2023) (where $r = 3$) that the optimisation always caps the r for monolithic IGUs, which is better for the weight but worse for the load sharing and geometric nonlinearity.

Table 2. Young's modulus for the PVB interlayer (Trosifol UltraClear) and the ionomer interlayer (SentryGlas Plus) at different temperatures for a 1-minute loading time. The data is obtained from the Trosifol technical data sheet (Kuraray 2024). The shear modulus is calculated from Young's modulus with Poisson's ratio of 0.49.

Temperature [°C]	Trosifol UltraClear [MPa]	SentryGlas Plus [MPa]
25°C	1.8	413
35°C	1.2	209
50°C	0.69	33.8

Therefore, choosing r is a trade-off between the weight and redundancy.⁴ Large thickness difference between t_1 and t_2 could imply optical distortions of some degree, but they are not considered in the current study. The total thickness of the directly loaded laminated glass must be larger than the total thickness of the indirectly loaded laminated glass but can only be twice as large. The interlayer thickness is chosen as 1.52 mm.

5.2. Optimized laminated IGUs

The optimised thicknesses are shown in Tables 4 and 5 for the 2.5 kPa and 15.0 kPa design loads, respectively. First, for the 2.5 kPa load and the small sizes, all the thicknesses are at their lower limit (4 mm) regardless of the temperature. For a larger window size, the total minimum required thickness only grows by 2 mm at maximum when the temperature increases (for a given window size). That is, for the typical 2.5 kPa load, the thickness may well be chosen for a 25°C temperature since the increase in the temperature does not significantly increase the required minimum thickness. A similar trend can be observed also for the higher design load of 15.0 kPa. Looking at the thicknesses between the two interlayer materials (PVB and SGP) at a given temperature for large windows and large loads, it is very beneficial to use the stiffer SGP interlayer. The difference varies between 0% and 26%. Large potential weight savings can be achieved using an SGP interlayer instead of a PVB interlayer.

5.3. Response

The maximum principal stress of each glass pane, the maximum deflection, and the load sharing percentage for the optimised thicknesses are presented in Tables 6 and 7 for the 2.5 kPa and 15.0 kPa design loads, respectively. The limiting response values are bolded and colours are used to indicate which criterion is the limiting one. In cases where all the thicknesses are at the lower limit of 4 mm, the stress and deflection limits are not reached. Only in three of the cases is the stress a limiting factor. In two other cases, the stress and the deflection are both limiting factors. Deflection is the limiting factor in the remaining cases. One can also observe that with the PVB interlayers, the stresses are quite high in both laminated glass panes. The load sharing percentage is close to 50% when the two laminated glass panes have almost equal total thickness. It drops significantly as the ratio between the total thicknesses decreases. Hence, the optimisation leads to a configuration where the directly loaded laminated glass carries most of the load, and the other laminated glass is as thin as possible. Further, the interlayer stiffness does not seem to influence the load sharing significantly. It is more a function of the thickness configuration and size as was found by Heiskari et al. (2023).

This can further be demonstrated by considering a case, say a 3500×3500 window subjected to a 15 kPa load and having a thickness configuration of 21, 18, 12, and 8 mm for t_1 , t_2 , t_3 , and t_4 , respectively (optimised thickness for PVB at 25°C). Young's modulus for the interlayer varies from 1 MPa to 413 MPa at intervals of 2 MPa. The influence of the interlayer stiffness on the load sharing

Table 3. Design constraints.

Design constraint	Symbol	Value
Maximum principal stress	$\sigma_{+,d}$ [MPa]	40
Maximum deflection	δ_d [–]	100
Thickness ratio	r [–]	2
Thickness lower limit	t_{lower} [mm]	4
Thickness upper limit	t_{upper} [mm]	varied

Table 4. Optimized thicknesses with maximum principal stress and maximum deflection criterion for a 2.5 kPa design load.

Temperature [°C]	25		35		50	
Material	PVB	SGP	PVB	SGP	PVB	SGP
$a = 1500 \text{ mm}$ $b = 1500 \text{ mm}$						
t_1 [mm]	4 (1)	4 (1)	4 (1)	4 (1)	4 (1)	4 (1)
t_2 [mm]	4	4	4	4	4	4
t_3 [mm]	4 (1)	4 (1)	4 (1)	4 (1)	4 (1)	4 (1)
t_4 [mm]	4	4	4	4	4	4
Total [mm]	16 [1]	16 [1]	16 [1]	16 [1]	16 [1]	16 [1]
$a = 2500 \text{ mm}$ $b = 1500 \text{ mm}$						
t_1 [mm]	5 (1.25)	4 (1)	6 (1.5)	4 (1)	7 (1.75)	4 (1)
t_2 [mm]	4	4	4	4	4	4
t_3 [mm]	5 (1.25)	4 (1)	4 (1)	4 (1)	5 (1.25)	4 (1)
t_4 [mm]	4	4	4	4	4	4
Total [mm]	18 [1]	16 [1]	18 [1.25]	16 [1]	20 [1.22]	16 [1]
$a = 3500 \text{ mm}$ $b = 3500 \text{ mm}$						
t_1 [mm]	8 (1.33)	6 (1)	9 (1.5)	8 (1.6)	9 (1.29)	8 (1.6)
t_2 [mm]	6	6	6	5	7	5
t_3 [mm]	7 (1.75)	4 (1)	7 (1.75)	4 (1)	7 (1.75)	4 (1)
t_4 [mm]	4	4	4	4	4	4
Total [mm]	25 [1.27]	20 [1.5]	26 [1.36]	21 [1.63]	27 [1.45]	21 [1.63]

Notes: The resulting thickness ratios t_1/t_2 and t_3/t_4 are presented in the parenthesis after t_1 and t_3 , respectively. The thickness ratio $(t_1 + t_2)/(t_3 + t_4)$ is presented in brackets after the total thickness.

Table 5. Optimized thicknesses with maximum principal stress and maximum deflection criterion for a 15 kPa design load.

Temperature [°C]	25		35		50	
Material	PVB	SGP	PVB	SGP	PVB	SGP
$a = 1500 \text{ mm}$ $b = 1500 \text{ mm}$						
t_1 [mm]	11 (1.83)	8 (2)	11 (1.57)	8 (2)	12 (2)	6 (1)
t_2 [mm]	6	4	7	4	6	6
t_3 [mm]	5 (1.25)	4 (1)	5 (1.25)	4 (1)	5 (1.25)	5 (1.25)
t_4 [mm]	4	4	4	4	4	4
Total [mm]	26 [1.89]	20 [1.5]	27 [2]	20 [1.25]	27 [2]	21 [1.33]
$a = 2500 \text{ mm}$ $b = 1500 \text{ mm}$						
t_1 [mm]	16 (2)	11 (1.57)	16 (2)	11 (1.57)	16 (1.78)	11 (1.57)
t_2 [mm]	8	7	8	7	9	7
t_3 [mm]	7 (1.4)	6 (1.5)	7 (1.4)	6 (1.2)	7 (1)	7 (1.75)
t_4 [mm]	5	4	5	5	7	4
Total [mm]	36 [2]	28 [1.8]	36 [2]	29 [1.63]	39 [1.79]	29 [1.63]
$a = 3500 \text{ mm}$ $b = 3500 \text{ mm}$						
t_1 [mm]	21 (1.17)	15 (1)	24 (1.5)	16 (1.14)	26 (1.73)	19 (1.58)
t_2 [mm]	18	15	16	14	15	12
t_3 [mm]	12 (1.5)	8 (1.14)	13 (1.86)	9 (1.5)	14 (2)	11 (1.83)
t_4 [mm]	8	7	7	6	7	6
Total [mm]	59 [1.95]	45 [2]	60 [2]	45 [2]	62 [1.95]	48 [1.82]

Notes: The resulting thickness ratios t_1/t_2 and t_3/t_4 are presented in the parenthesis after t_1 and t_3 , respectively. The thickness ratio $(t_1 + t_2)/(t_3 + t_4)$ is presented in brackets after the total thickness.

is shown on the left-hand side of Figure 12. It drops slightly at the beginning but then remains constant at 14%. If the total thickness of the glass panes is kept almost the same but is distributed evenly between the glass panes, i.e. all panes are 15 mm thick, then the load sharing is much higher, as can be seen on the right-hand side of Figure 12. However, the load sharing remains constant at 47% after the initial small drop. It should be noted that this latter configuration is not feasible because the total thickness of the directly loaded laminated glass is too thin to fulfill the design criteria. It can be concluded that the interlayer does not significantly influence the load sharing.

The through-thickness stress distribution is plotted to show the difference between the optimised IGUs for the PVB and SGP interlayers. A square IGU with a 3500 mm side length is chosen for this demonstration. The design load is 15.0 kPa, and the thicknesses are as optimised in Table 5. Normal stresses in the x - and y -direction (which are identical to each other) are plotted in the middle of the IGU, even though the maximum value of the stress may not

be located there. The results are shown in Figure 13. The monolithic stress distribution is also plotted with a blue line for comparison because it pushes towards this behaviour as the interlayer becomes stiffer. First, it is obvious that the laminated glass panes are in partial shear transfer mode. The stresses are naturally higher for the directly loaded laminated glass as it is thicker than the other one. The SGP interlayer shows weaker zigzag behaviour, as expected. The stress distribution with the SGP interlayer in glass panes one and three is equivalent to the monolithic stress distribution. Further, the maximum compressive and maximum tensile stresses are almost the same for the zigzag and monolithic cases. Clearly, including the zigzag behaviour is important, especially with the less stiff interlayers because the tensile stresses are high on the bottom of both panes of laminated glass (locations (1,2) and (1,4), and (2,1) and (2,4)). Pane one may even have higher tensile stress than pane two, as shown with PVB at 50°C.

By observing the stress difference at the top and bottom of the interlayer, we can determine how effective the interlayer is, that

Table 6. Largest maximum principal stress and maximum deflection (in parenthesis) of the optimised cases (Table 9) for a design load of 2.5 kPa.

$a = 1500 \text{ mm } b = 1500 \text{ mm [40 MPa, 15 mm]}$						
Temperature [°C]	25		35		50	
Material	PVB	SGP	PVB	SGP	PVB	SGP
t_1 [MPa]	9.1	5.2	10.1	5.1	11.4	4.6
t_2 [MPa]	11.0 (10.0 mm)	9.3 (5.1 mm)	11.1 (10.6 mm)	9.4 (5.2 mm)	11.6 (11.4 mm)	10.0 (5.9 mm)
t_3 [MPa]	8.6	4.8	9.5	4.7	10.7	4.2
t_4 [MPa]	10.7 (9.6 mm)	8.6 (4.7 mm)	10.9 (10.3 mm)	8.7 (4.8 mm)	11.0 (11.1 mm)	9.3 (5.5 mm)
Load sharing [%]	49	48	49	48	49	48
$a = 2500 \text{ mm } b = 1500 \text{ mm [40 MPa, 15 mm]}$						
t_1 [MPa]	11.2	7.2	13.0	7.0	13.9	6.3
t_2 [MPa]	14.1 (14.4 mm)	15.7 (9.9 mm)	13.5 (13.8 mm)	15.8 (10.1 mm)	12.1 (14.2 mm)	16.2 (10.9 mm)
t_3 [MPa]	10.6	6.9	8.3	6.8	10.3	5.9
t_4 [MPa]	13.9 (14.1 mm)	15.2 (9.5 mm)	11.3 (13.2 mm)	15.3 (9.7 mm)	10.9 (13.7 mm)	15.7 (10.6 mm)
Load sharing [%]	49	49	31	49	36	49
$a = 3500 \text{ mm } b = 3500 \text{ mm [40 MPa, 35 mm]}$						
t_1 [MPa]	18.1	15.2	19.1	14.0	19.6	13.4
t_2 [MPa]	15.7 (34.3 mm)	19.0 (35.0 mm)	14.6 (34.0 mm)	19.0 (33.3 mm)	16.0 (34.4 mm)	19.1 (34.2 mm)
t_3 [MPa]	17.7	12.8	17.9	11.4	19.0	9.9
t_4 [MPa]	13.1 (33.5 mm)	15.6 (33.4 mm)	12.0 (32.9 mm)	13.9 (31.7 mm)	11.3 (33.2 mm)	13.7 (32.5 mm)
Load sharing [%]	38	31	35	27	33	27

Notes: The load sharing percentage is calculated as the ratio of the cavity pressure to the applied pressure. The maximum stress and deflection criteria are inside the brackets after the IGU planar dimensions. The bolded response indicates the activated criterion. Furthermore, the cell colours green, red, and orange indicate if the deflection, stress, or both criteria, respectively, are activated.

Table 7. Largest maximum principal stress and maximum deflection (in parenthesis) of the optimised cases (Table 10) for a design load of 15.0 kPa.

$a = 1500 \text{ mm } b = 1500 \text{ mm [40 MPa, 15 mm]}$						
Temperature [°C]	25		35		50	
Material	PVB	SGP	PVB	SGP	PVB	SGP
t_1 [MPa]	29.8	17.9	29.7	18.0	32.7	16.4
t_2 [MPa]	25.4 (14.8 mm)	37.5 (13.9 mm)	25.6 (14.9 mm)	37.7 (14.1 mm)	22.5 (14.8 mm)	34.7 (14.8 mm)
t_3 [MPa]	16.1	13.3	16.4	13.0	16.4	13.2
t_4 [MPa]	15.9 (13.3 mm)	23.6 (12.5 mm)	14.9 (13.4 mm)	23.8 (12.7 mm)	13.8 (13.3 mm)	25.4 (13.3 mm)
Load sharing [%]	17	26	16	27	14	32
$a = 2500 \text{ mm } b = 1500 \text{ mm [40 MPa, 15 mm]}$						
t_1 [MPa]	33.0	13.6	36.5	12.9	37.5	16.6
t_2 [MPa]	25.6 (14.0 mm)	39.9 (12.3 mm)	25.2 (15.0 mm)	38.6 (12.1 mm)	25.3 (14.9 mm)	39.6 (13.8 mm)
t_3 [MPa]	11.9	9.5	13.0	9.5	13.5	10.2
t_4 [MPa]	15.7 (13.1 mm)	22.6 (11.5 mm)	15.3 (14.0 mm)	23.2 (11.2 mm)	17.7 (13.9 mm)	25.2 (12.8 mm)
Load sharing [%]	14	17	13	21	16	22
$a = 3500 \text{ mm } b = 3500 \text{ mm [40 MPa, 35 mm]}$						
t_1 [MPa]	25.5	20.3	27.8	20.3	29.6	20.5
t_2 [MPa]	30.4 (34.8 mm)	38.9 (34.4 mm)	27.6 (34.8 mm)	39.1 (34.4 mm)	24.9 (34.7 mm)	37.6 (34.0 mm)
t_3 [MPa]	18.8	14.3	19.6	14.2	20.0	14.0
t_4 [MPa]	17.6 (32.4 mm)	20.2 (32.5 mm)	16.0 (32.4 mm)	20.6 (32.6 mm)	14.3 (32.2 mm)	21.7 (32.3 mm)
Load sharing [%]	18	16	18	16	18	19

Notes: The load sharing percentage is calculated as the ratio of the cavity pressure to the applied pressure. The maximum stress and deflection criteria are inside the brackets after the IGU planar dimensions. The bolded response indicates the activated criterion. Furthermore, the cell colours green, red, and orange indicate if the deflection, stress, or both criteria, respectively, are activated.

is, how well the interlayer transfers the shear. First, the ‘stress jump’ is calculated as:

$$\sigma_{j,i} = \sigma_{i,3} - \sigma_{i,2} \quad (10)$$

where subscript $i = 1, 2$ indicates the laminated glass number, j is

the jump, and 2 and 3 are the stress values at the top and bottom of the interlayer, respectively. These locations are shown in Figure 13. Next, this jump is scaled with the interlayer thickness:

$$R_{i,int} = \frac{t_{int}}{\sigma_{i,jump}}. \quad (11)$$

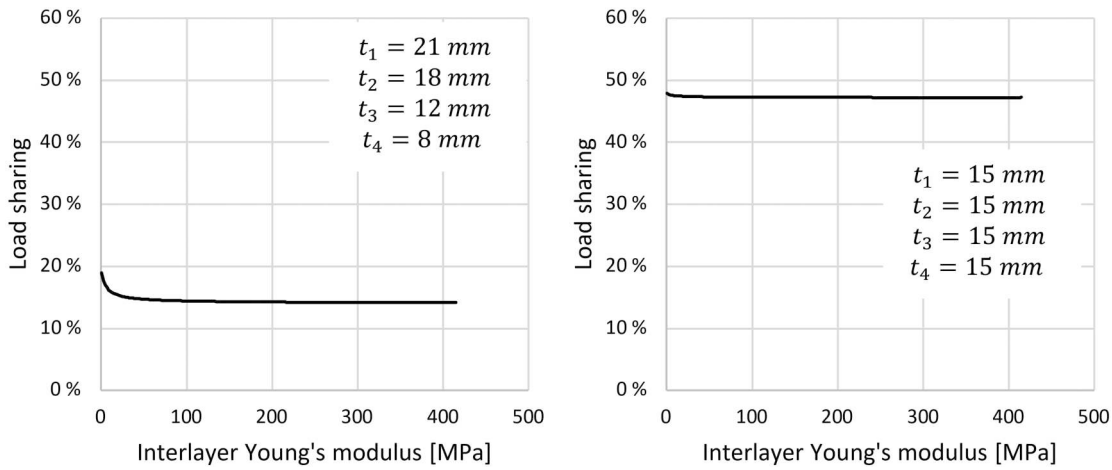


Figure 12. Load sharing percentage (ratio of cavity pressure to applied load) for 3500×3500 laminated IGU subjected to 15.0 kPa load with two different thickness configurations. Left-hand side: optimised thickness for 25°C PVB interlayer. Right-hand side: a case with equally thick glass panes.

Then the ratio of the monolithic thickness to monolithic stress (blue line in Figure 13) is calculated:

$$R_{i,mono} = \frac{t_{i+(i-1)} + t_{2i} + t_{int}}{abs(\sigma_{i,1} - \sigma_{i,4})}. \quad (12)$$

Finally, the effectivity of the laminated glass can be obtained by comparing these two ratios:

$$H_i = \frac{R_{i,int}}{R_{i,mono}}. \quad (13)$$

The results are shown in Table 8. Clearly, the SGP interlayer is more effective than the PVB interlayer. The effectivity drops as the temperature increases. It is better to make the panes in the laminated glass equally thick with the SGP interlayer. For example, the thicknesses of the SGP interlayer at 25°C in the first laminated glass are $t_1 = 15$ mm and $t_2 = 15$ mm. These could be changed to 17 mm and 13 mm, respectively, without changing the overall response significantly, but the effectivity is lowered. On the other hand, the shear transfer with the PVB interlayer is far lower anyway, so it is better to make the directly loaded glass panes, i.e. t_1 and t_3 , much thicker so they carry most of the load. The optimisation has done exactly that (Table 5).

5.4. Comparison with classification rules

First, if the window has laminated glass, the monolithic thickness is used as a baseline thickness to determine the equivalent laminated thickness (Equation (A9)). The second thing to consider is the allowed minimum glass thickness. For DNV (2022), these are either 6, 8, or 10 mm, depending on the window size and location. For the laminated glass, the individual thickness of any pane must not be smaller than 4 mm. Currently, the smallest thicknesses (to our knowledge) on a ship for a large laminated IGU are 6, 6, 6, and 6 mm. However, the smallest total thickness for a laminated IGU is 16 mm in this study (i.e. 4 mm for each glass pane).

The determination of the laminated glass thickness is shown in the appendices. Only the Bureau Veritas (BV 2022) formulation allows for a user-defined value of the interlayer shear modulus. Lloyd's Register (LR 2022) has a few shear transfer coefficients depending on the load type and interlayer. For comparison, only 25°C and 1 min loading are used in the BV formulation, and the shear transfer coefficients of 0.3 and 0.7 are used in the LR formulation for the PVB and SGP interlayers, respectively. For the IGUs,

the directly loaded laminated glass is calculated according to the rules, and the indirectly loaded laminated glass is chosen as the minimum possible. However, the total thickness of the indirectly loaded laminated glass cannot be more than two times smaller than the total thickness of the directly loaded pane. This is not specified in the rules but is simply used to allow a fairer comparison between the methods.

The results are shown in Tables 9 and 10 for design loads of 2.5 kPa and 15.0 kPa, respectively. The optimised results for 25°C and 1 min loading time are also shown in the last column. First, the BV and LR rules are quite similar. The BV rules result in slightly thinner solutions for the SGP interlayers than the LR rules do because they allow high shear transfer. However, this difference is only visible for the higher design load. For the PVB interlayer, BV and LR are almost the same, with minor differences. The DNV rules result in very thick glass panes compared to other methods, especially for a higher design load. Second, there is no big difference in the PVB interlayer between the BV (or LR) rules and the optimised thicknesses. In one case, the class rules provide up to a 1 mm thinner configuration than the optimisation. Generally, however, the optimisation results in a 1 mm to 3 mm thinner configuration. On the other hand, the difference is more significant for the SGP interlayer and the higher design load. Depending on the size, the optimisation configuration is 2 mm to 8 mm thinner than the *thinnest* class rule configuration. All these correspond to weight savings of –6 to 15% with respect to the class rules. While the class results can be good from an engineering perspective, they do not account for the underlying physical principles, i.e. they neglect the geometric nonlinearity and the load sharing.

5.5. Recent ISO 11336-1 updates

The ISO 11336-1:2012 (ISO 2012) standard was recently updated to a 2023 version (ISO 2023) where the main updates relating to the current study are as follows:

- (1) A deflection limit has been introduced – $a/50$ mm.
- (2) The minimum characteristic failure strength of fully tempered glass has been lowered to 120 MPa from 160 MPa.
- (3) The strength safety factor has been lowered from 4 to 3.
- (4) The design load time for interlayer material property definition has been lowered from 60 seconds to 10 seconds.

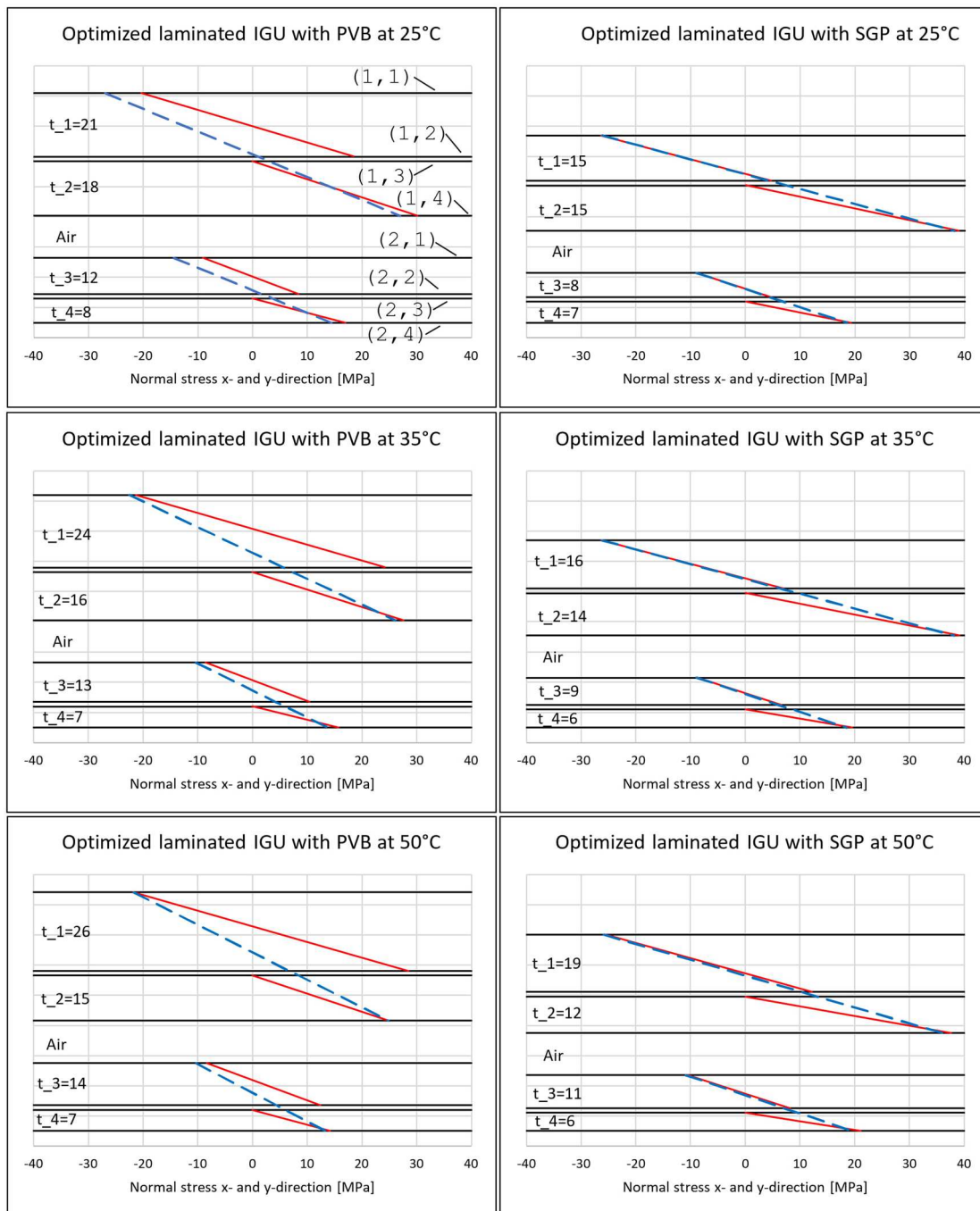


Figure 13. Through-thickness normal stress distribution for the glass panes at the geometric midpoint of the IGU. The thicknesses are optimised for a 3500×3500 IGU subjected to a 15.0 kPa design load. Each row has a certain loading temperature, and the left-hand side column is PVB and the right-hand side column SGP. The blue line is the stress distribution if the laminated glass were of monolithic construction (i.e. the interlayer has the same properties as the glass). $i = 1, 2$ and $k = 1, 2, 3, 4$ indicate the layer position. For example, (1, 2) is the layer between the first glass pane and the interlayer in the first laminated glass. (This figure is available in colour online.)

Points (2) and (3) result in the same design strength of 40 MPa as did the previous version. Point (4) makes the design stiffness of the interlayer larger, but it is not implemented in the current study, as the classification rules still use 60 seconds. Point (1) is the most relevant change to the study because a deflection limit of $b/100$ was used in optimising the thicknesses in this chapter. In the standard, a is the longer rectangular side, but when $a \geq 1.4b$, a is given as $1.4b$. Implementing that to the cases in this study means that the allowed maximum deflections would be 30 mm, 42 mm, and 70 mm for $a = b = 1500$ mm, $a = 2500$, $b = 1500$ mm, and $a = b = 3500$ mm, respectively. These appear to influence only the direct calculation

methods (such as FEM analysis), as the monolithic thickness equation as per standard has not been updated.

To have an idea what such limits mean, all the cases in Tables 4 and 5 were optimised again by using the $a/50$ mm criterion. Interestingly, the new deflection limit was never reached (it only reached 70% of it at most), and all the designs were limited by the 40 MPa stress criterion. That is, all the thicknesses in Table 4 for the 2.5 kPa loads can be replaced with 4 mm (except for 3500×3500 PVB with 1.2 MPa and 0.69 MPa interlayer stiffnesses). This lightens the design from 0% (already at the minimum of 16 mm total thickness) up to 40% by using the $a/50$ mm criterion over the $b/100$ criterion.

Table 8. Effectivity of 3500×3500 optimised laminated IGUs at three temperatures and two different interlayer materials.

Material Temperature [°C]	PVB			SGP		
	25	35	50	25	35	50
H_1 [%]	11	7	6	67	45	23
H_2 [%]	24	16	13	55	39	30

Notes: The applied load is 15.0 kPa. The percentage is calculated from the thicknesses and stress values shown in Figure 13 using Equation (13).

On the other hand, the weight difference for the 15.0 kPa design load varies from 0% (some designs were already at the stress limit) up to 30% between the two deflection criteria. These results further demonstrate (as previously discussed by Heiskari et al. 2022b, 2023) how important an allowable deflection limit can be. However, there is no clear physical reasoning for any of the limits (not even in the updated ISO standard). For example, the prEN 13474-3 standard (prEN 2009) suggested 'span'/65 mm or 50 mm (whichever is the lower value) to ensure that the glass panes are not excessively flexible under loads, which can cause alarm to building users. Clearly, choosing the limit is not a trivial task to do, and it will require future studies.

5.6. Comments on the optimisation

The PSO swarm size was set to 100. That is, each iteration included 100 analyses. The optimum was found typically in 8 to 12 iterations, which included 4 iterations that did not improve the weight (stopping criterion). One ANSYS analysis took anywhere between 2 seconds to 2 minutes, depending on the IGU configuration (size and thickness) and the load level. One optimisation routine could take up to 2 hours using a home desktop PC (16.0 GB RAM and AMD Ryzen 5 5600x 6-core processor).

6. Discussion

When calculating the required minimum glass pane thickness of ship windows, it is important that the method used considers the physical effects that occur. First, this means accounting for geometric nonlinearities. The classification society rules are still limited to the linear approach. The difference between the linear and nonlinear method for a large, laminated glass (not an IGU) subjected to a large load is shown in Figure 14. When the class rules are compared with each other for monolithic glass panes, they are practically identical (Heiskari et al. 2022a). Second, the load sharing between the glass panes due to the enclosed cavity in IGUs significantly increases the load-bearing capacity of the windows. The classification rules are identical also in the sense that their methods cannot yet consider the load sharing effect.⁵ Finally, shear transfer plays an important role. There are clearly differences in how it is treated in different classification rules. The most flexible approach is that of Bureau Veritas (BV 2022), which is equivalent to that given by the ISO 11336-1 standard (ISO 2012, 2023), where one can freely determine the degree of the shear transfer. On the other hand, Lloyd's Register has a few discrete predetermined values, while the DNV (2022) rules do not really consider the shear transfer. However, the DNV rules do mention that the ISO 11336-1 method can be used, providing certain criteria are met. In that light, the class rules in this study are almost at the same level as each other.

However, looking at Figure 14, it is clear that analysing the windows on a linear basis can heavily underestimate the deflections and stresses. If the glass pane thicknesses are kept constant and only the interlayer properties are changed (Figure 14), then the importance of nonlinearity is more significant for the PVB interlayer. On the

Table 9. Required minimum glass pane thicknesses for laminated IGUs according to the different classification societies for 2.5 kPa design load at 25°C.

Class Material	BV		LR		DNV		Opt.	
	PVB	SGP	PVB	SGP	PVB	SGP	PVB	SGP
$a = 1500 \text{ b} = 1500 \text{ mm}$								
t_{mono} [mm]	6.3		6.4		6.3		—	
t_1 [mm]	4	4	4	4	5		4	4
t_2 [mm]	4	4	4	4	5		4	4
t_3 [mm]	4	4	4	4	4		4	4
t_4 [mm]	4	4	4	4	4		4	4
Total [mm]	16	16	16	16	18		16	16
$a = 2500 \text{ b} = 1500 \text{ mm}$								
t_{mono} [mm]	8.7		8.6		8.7		—	
t_1 [mm]	5	4	5	4	7		5	4
t_2 [mm]	4	4	5	4	6		4	4
t_3 [mm]	4	4	4	4	4		5	4
t_4 [mm]	4	4	4	4	4		4	4
Total [mm]	17	16	18	16	21		18	16
$a = 3500 \text{ b} = 3500 \text{ mm}$								
t_{mono} [mm]	14.7		15.0		14.7		—	
t_1 [mm]	9	7	9	8	12		8	6
t_2 [mm]	8	7	8	7	10		6	6
t_3 [mm]	5	4	5	4	6		7	4
t_4 [mm]	4	4	4	4	5		4	4
Total [mm]	26	22	26	23	33		25	20

Notes: The optimised results are shown in the last column. For DNV, there is no distinction between different interlayers.

Table 10. Required minimum glass pane thicknesses for laminated IGUs according to the different classification societies for 15.0 kPa design load at 25°C.

Class Material	BV		LR		DNV		Opt.	
	PVB	SGP	PVB	SGP	PVB	SGP	PVB	SGP
$a = 1500 \text{ b} = 1500 \text{ mm}$								
t_{mono} [mm]	15.4		15.7		15.4		—	
t_1 [mm]	9	7	9	8	11		11	8
t_2 [mm]	9	7	9	8	11		6	4
t_3 [mm]	5	4	5	4	6		5	4
t_4 [mm]	4	4	4	4	5		4	4
Total [mm]	27	22	27	24	33		26	20
$a = 2500 \text{ b} = 1500 \text{ mm}$								
t_{mono} [mm]	21.3		21.0		21.3		—	
t_1 [mm]	13	10	12	11	16		16	11
t_2 [mm]	13	10	12	10	15		18	7
t_3 [mm]	7	6	6	6	8		7	6
t_4 [mm]	6	4	6	5	8		5	4
Total [mm]	40	30	36	32	47		36	28
$a = 3500 \text{ b} = 3500 \text{ mm}$								
t_{mono} [mm]	36.0		36.7		36.0		—	
t_1 [mm]	20	18	21	20	26		21	15
t_2 [mm]	20	17	21	18	26		18	15
t_3 [mm]	10	9	11	10	13		12	8
t_4 [mm]	10	9	11	9	13		8	7
Total [mm]	60	53	64	57	78		59	45

Notes: The optimised results are shown in the last column. For DNV, there is no distinction between different interlayers.^o

other hand, if the glass pane thickness is determined for a certain interlayer so that no maximum deflection and stress criteria are violated, like in this study, then the difference between the nonlinear FEM and the classification rule method is larger for the stiffer SGP interlayer than for the PVB interlayer. This can be observed in Table 10. The reason is that the stiffer SGP interlayer allows for thinner glass panes, which promotes the von Kármán strains, i.e. the geometric nonlinearity. If the PVB interlayer is used, then the directly loaded glass pane becomes thicker and carries most

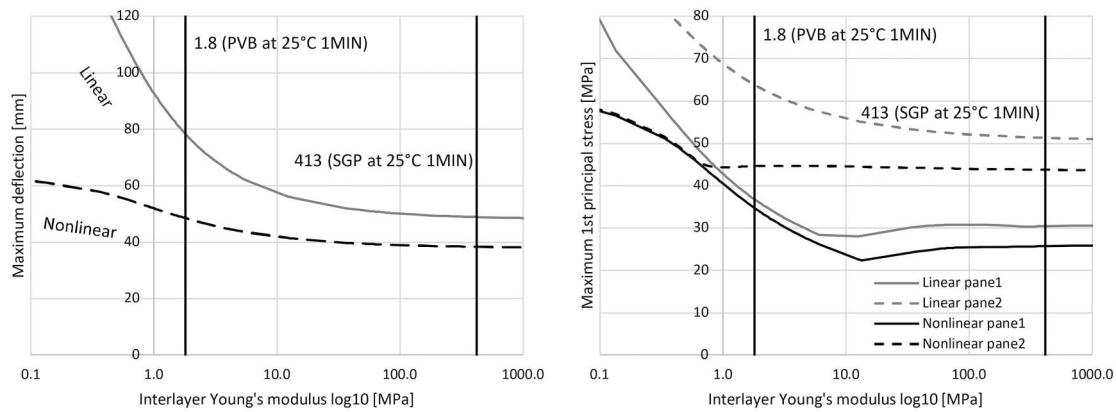


Figure 14. Deflection and maximum principal stress comparison of rectangular laminated glass (not an IGU) with a side length of 3500 mm subjected to a 15 kPa uniformly distributed load on a linear and nonlinear basis. The thickness of the glass panes and the interlayer are 20 mm and 1.52 mm, respectively. The Young's modulus of the interlayer is varied. The vertical lines represent the typical interlayer conditions for PVB and SGP interlayers at 25°C and 1-minute loading. Pane 1 is the directly loaded glass pane. The results are obtained from FEM analysis.

of the load through bending. The BV and the LR class rules result in thickness configurations that are close to the optimised configurations, as can be seen in Tables 9 and 10, even though they neglect the load sharing and geometric nonlinearity. The difference between the BV and optimised thicknesses vary from -6% to 9%, and 2% to 15% for 2.5 kPa and 15.0 kPa design loads, respectively. However, the comparison is problematic as the classification rules use only stress criterion while a $b/100$ mm deflection criterion was used in optimisation, which was the limiting criterion in most of the cases. By using a deflection limit of $a/50$ (as given in the new ISO 2023 113361-1 standard), which did not activate in the presented case studies and the stress was the limiting criterion, the difference to the class varies from 0% to 38%, and 10% to 33% for 2.5 kPa and 15.0 kPa design loads, respectively. Hence, the chosen design constraints play a major role in the thickness optimisation.

By comparing only the PVB and SGP interlayers together (no class), it was found that it is better to use equally thick glass panes in laminated glass with the stiffer SGP interlayer because then the stress jump, i.e. the zigzag behaviour, becomes smaller. This increases the effectiveness of the interlayer. On the other hand, with less stiff PVB interlayers, the directly loaded glass pane in the laminated glass should be much thicker so it can carry most of the load on its own. This is because the interlayer cannot transfer the load as effectively. This becomes apparent from Table 5, where one can observe in how much thicker t_1 than t_2 the optimisation algorithm converges. Then, the maximum value of the maximum principal stress is found at the bottom surface of the t_1 glass pane, while it is at the bottom of the t_2 glass pane for the SGP case. Because of the very thick t_1 glass pane in the PVB case, deflection limit is always activated before the stress limit. In fact, the stress is always 10 to 15 MPa from the 40 MPa limit, as shown in Table 7. On the other hand, the stress becomes the limiting criterion for the SGP cases with higher design load and larger sizes. With the lower design load and small window sizes, the minimum allowable glass pane thickness of 4 mm is limiting the design. That is, optimisation would have reduced the thickness even further. However, many of the thin IGUs in modern cruise ships are built with 6 mm glass panes and SGP interlayers. Looking at the optimised thicknesses in Table 4 and their response in Table 6, it is clear that 4 mm can be enough to fulfill the design criteria in this study. Further, at least for smaller windows, a PVB interlayer seems to be sufficient. This offers potential cost savings. On the other hand, an SGP interlayer provides potential weight savings with larger windows.

It is clear that the FEM analysis is very useful, as it allows inclusion not only of the geometric nonlinearity but also of the load sharing and shear transfer. Furthermore, it allows the window shape and boundary conditions to be freely determined. This offers a significant advantage over analytical methods (e.g. class rule methods), as windows in ships can have, for example, very irregular triangular shapes, and the bonding of windows to the steel frame does not follow the typically assumed simply-supported boundary condition. Therefore, it is recommended to determine the glass pane thickness based on the FEM when lightweight windows are designed. Finally, it should be noted that these findings relate to windows that are not expected to encounter wave loads. This is because the dynamic loads, such as waves, on windows and resulting load magnitudes have not been studied well.

7. Conclusions

This paper studied the bending behaviour of insulating glass units that consist of laminated glass. Their response was obtained from nonlinear finite element method (FEM) analysis. Using the FEM analysis allowed for the inclusion of geometric nonlinearities of the glass panes, shear transfer in the laminated glass, and load sharing in the unit. The goal was to calculate the required minimum glass pane thickness for the two most used interlayer materials, three different window sizes, and two different design loads so that no structural design criteria were violated. These were then compared to the minimum thicknesses set by the classification society rules. The motivation for the study was to reduce the weight of windows in ships and find potential cost savings.

The results show that with smaller windows and a small design load, it makes no practical difference whether the glass pane thicknesses are chosen based on nonlinear FEM analysis or classification rules. This is because the allowed minimum glass pane thickness has been reached. With these conditions, the interlayer material is also irrelevant, which opens potential cost savings. The difference becomes more important as the design load and window size increase. First, one can save weight by choosing the stiffer SGP interlayer material over PVB. Second, the difference between the nonlinear FEM and the class rule method becomes more significant. That is, potential weight savings are available. However, at what point do the FEM analysis and class rule method deviate from each other heavily depends on the used design constraints.

The FEM offers far more design freedom regarding loading conditions, boundary conditions, window shape and construction, and analysis type than analytical methods do (e.g. class rule methods).

These are all important aspects, as an accurate response of the structure must be obtained already in the early design phases of the ships when different design variants are explored. Further, finding the potential weight and cost savings is not possible with simple design methods, as the results have shown. For these reasons, it is recommended to use the FEM when analysing ship windows and optimising them for lightweight designs.

This study had a single objective optimisation routine that assumed that reducing the thickness of the glass panes has only a positive effect. However, it also affects the sound insulation and thermal insulation properties, and the material and building costs were not considered appropriately. It is possible to run a multi-objective optimisation where these aspects are considered. However, such an optimisation is more complex than presented here but is worth exploring. The choice of interlayer material affects the noise and vibration properties of the laminated glass. If windows are located in areas where significant vibration is expected, a vibration study might be necessary to check that the window's natural frequency is not too close to the excitation frequency. However, this may require details that are not available in the concept design phase of the ship. Furthermore, the load was quasi-static; it is possible to have dynamic loads that can break the windows. Therefore, the effect of dynamic loading on laminated IGU behaviour should be studied in the future. Finally, the results are based on numerical studies; future experimental studies of large laminated IGUs under large deflection will add further understanding.

Notes

1. These materials have different noise and vibration properties. For example, PVB may provide better sound transmission loss as a softer material. However, the present study does not consider these aspects.
2. The effect of the ambient pressure and temperature changes on the cavity pressure of the IGU, i.e. climate loads (Buddenberg et al. 2016; Kozłowski et al. 2023), are neglected in this study.
3. Note that the used PSO algorithm is the same as in the Authors' earlier studies (Heiskari et al. 2022b, 2023), but it is presented here again for clarification purposes.
4. Redundancy, in this case, means that if either glass pane breaks in the laminated glass (no shear transfer), or if either laminated glass breaks completely (no load sharing), the remaining glass panes have better chances to carry the load on their own.
5. The new ISO (2023) 11336-1 standard acknowledges the significance of load sharing and suggests designers consider it according to simple equations presented in SFS-EN (2019) 16612 standard.

Acknowledgments

The work is part of the carbon-neutral lightweight ship structures using advanced design, production, and life-cycle Services (CaNeLis) project within the scope of Climate-Neutral Cruise Ship (NECOLEAP) and Sustainable Manufacturing Finland roadmaps. All financial support is greatly appreciated. Finally, Ari Niemelä, head of hull basic design at Meyer Turku Oy, is greatly acknowledged for providing helpful comments and feedback.

Data availability statement

Data will be made available on request.

Disclosure statement

No potential conflict of interest was reported by the author(s).

Funding

The corresponding author was supported by the School of Engineering at Aalto University. Further, the research presented in this paper has received funding from Business Finland under grant No. 3409/31/2022.

ORCID

Janne Heiskari  <http://orcid.org/0000-0003-1398-1605>

References

- Andric J, Kitarovic S, Radolovic V, Prebeg P. 2019. Structural analysis and design of a car carrier with composite sandwich deck panels. *Ships Offshore Struct.* 14:171–186. doi: [10.1080/17445302.2018.1564536](https://doi.org/10.1080/17445302.2018.1564536)
- Andric J, Prebeg P, Andrisic J, Zanich V. 2020. Structural optimisation of a bulk carrier according to IACS CSR-BC. *Ships Offshore Struct.* 15:123–137. doi: [10.1080/17445302.2019.1589976](https://doi.org/10.1080/17445302.2019.1589976)
- ANSYS. 2024a. Ansys Mechanical APDL 2024 R1. Element Reference. Chapter 7: Element Library – HSFLD242 – 3D Hydrostatic Fluid.
- ANSYS. 2024b. Ansys Mechanical APDL 2024 R1. Element Reference. Chapter 7: Element Library – SHELL181 – 4-Node Structural Shell.
- ANSYS. 2024c. Ansys Mechanical APDL 2024 R1. Element Reference. Chapter 7: Element Library – SOLSH190 – 3D 8-Node Structural Solid Shell.
- Bostick CW. 2009. Architectural trends thru the looking glass. In: *Proceedings of the Glass Performance Days*, Tampere, Finland. p. 860–866.
- Buddenberg S, Hof P, Oechsner M. 2016. Climate loads in insulating glass units: comparison of theory and experimental results. *Glass Struct Eng.* 1:301–313. doi: [10.1007/s40940-016-0028-z](https://doi.org/10.1007/s40940-016-0028-z)
- BV. 2022. Bureau Veritas, Rules for the Classification of Steel Ships, Part B Hull and Stability, July.
- Clerc M, Kennedy J. 2002. The particle swarm -- explosion, stability, and convergence in a multidimensional complex space. *IEEE Trans Evol Comput.* 6:58–73. doi: [10.1109/4235.985692](https://doi.org/10.1109/4235.985692)
- DNV. 2022. Rules for Classification: Ships, Part 3 Hull, Chapter 12 Openings and closing appliances, July.
- Foraboschi P. 2012. Analytical model for laminated-glass plate. *Compos Part B Eng.* 43:2094–2106. doi: [10.1016/j.compositesb.2012.03.010](https://doi.org/10.1016/j.compositesb.2012.03.010)
- Foraboschi P. 2014. Optimal design of glass plates loaded transversally. *Mater Eng.* 62:443–458.
- Freitas D, Lopes LG, Morgado-Dias F. 2020. Particle swarm optimisation: a historical review up to the current developments. *Entropy.* 22(3):362. doi: [10.3390/e22030362](https://doi.org/10.3390/e22030362)
- Fricke W, Gerlach B. 2015. Effect of large openings without and with windows on the shear stiffness of side walls in passenger ships. *Ships Offshore Struct.* 10:256–271. doi: [10.1080/17445302.2014.912048](https://doi.org/10.1080/17445302.2014.912048)
- Fröling M, Persson K. 2013. Computational methods for laminated glass. *J Eng Mech.* 139:780–790. doi: [10.1061/\(ASCE\)JEM.1943-7889.0000527](https://doi.org/10.1061/(ASCE)JEM.1943-7889.0000527)
- Galuppi L, Manara G, Royer Carfagni G. 2013. Practical expressions for the design of laminated glass. *Compos Part B Eng.* 45:1677–1688. doi: [10.1016/j.compositesb.2012.09.073](https://doi.org/10.1016/j.compositesb.2012.09.073)
- Galuppi L, Manara G, Royer Carfagni G. 2014. Erratum and addendum to “practical expressions for the design of laminated glass” [compos. part b: eng. 45 (2013) 1677–1688]. *Compos Part B Eng.* 56:599–601. doi: [10.1016/j.compositesb.2013.08.075](https://doi.org/10.1016/j.compositesb.2013.08.075)
- Galuppi L, Royer-Carfagni G. 2012a. The effective thickness of laminated glass plates. *J Mech Mater Struct.* 7:375–400. doi: [10.2140/jomms](https://doi.org/10.2140/jomms)
- Galuppi L, Royer-Carfagni G. 2020. Betti's analytical method for the load sharing in double glazed units. *Compos Struct.* 235:111765. doi: [10.1016/j.compstruct.2019.111765](https://doi.org/10.1016/j.compstruct.2019.111765)
- Galuppi L, Royer-Carfagni GF. 2012b. Effective thickness of laminated glass beams: new expression via a variational approach. *Eng Struct.* 38:53–67. doi: [10.1016/j.engstruct.2011.12.039](https://doi.org/10.1016/j.engstruct.2011.12.039)
- Gerlach B, Fricke W. 2016. Experimental and numerical investigation of the behavior of ship windows subjected to quasi-static pressure loads. *Mar Struct.* 46:255–272. doi: [10.1016/j.marstruct.2016.02.001](https://doi.org/10.1016/j.marstruct.2016.02.001)
- Haldimann M, Luible A, Overend M. 2008. Structural use of Glass. IABSE, Zurich, Switzerland. doi: [10.2749/sed010](https://doi.org/10.2749/sed010)
- He M, Liu M, Wang R, Jiang X, Liu B, Zhou H. 2019. Particle swarm optimization with damping factor and cooperative mechanism. *Appl Soft Comput.* 76:45–52. doi: [10.1016/j.asoc.2018.11.050](https://doi.org/10.1016/j.asoc.2018.11.050)
- Heiskari J, Romanoff J, Laakso A, Ringsberg JW. 2022a. On the thickness determination of rectangular glass panes in insulating glass units considering the load sharing and geometrically nonlinear bending. *Thin-Walled Struct.* 171:108774. doi: [10.1016/j.tws.2021.108774](https://doi.org/10.1016/j.tws.2021.108774)
- Heiskari J, Romanoff J, Laakso A, Ringsberg JW. 2022b. Thickness optimization of insulating glass unit in cruise ships. In: *Practical design of ships and other floating structures*. Dubrovnik: Faculty of Mechanical Engineering and Naval Architecture, University of Zagreb; p. 910–924.
- Heiskari J, Romanoff J, Laakso A, Ringsberg JW. 2023. Influence of the design constraints on the thickness optimization of glass panes to achieve lightweight insulating glass units in cruise ships. *Mar Struct.* 89:103409. doi: [10.1016/j.marstruct.2023.103409](https://doi.org/10.1016/j.marstruct.2023.103409)

- ISO. 2012. 11336-1, Large yachts -- Strength, weathertightness and watertightness of glazed openings -- Part 1: Design criteria, materials, framing and testing of independent glazed openings, International Organization for Standardization, Geneva.
- ISO. 2023. 11336-1, Large yachts -- Strength, weathertightness and watertightness of glazed openings -- Part 1: Design criteria, materials, framing and testing of independent glazed openings, International Organization for Standardization, Geneva.
- Kennedy J, Eberhart R. 1995. Particle swarm optimization. In: Proceedings of ICNN'95 -- International Conference on Neural Networks, Perth, WA, Australia. Vol. 4. p. 1942–1948. doi: [10.1109/ICNN.1995.488968](https://doi.org/10.1109/ICNN.1995.488968)
- Kozłowski M, Respondek Z, Wiśniowski M, Cornik D, Zemła K. 2023. Experimental and numerical simulations of climatic loads in insulating glass units by controlled change of pressure in the gap. Appl Sci. 13:1269. doi: [10.3390/app13031269](https://doi.org/10.3390/app13031269)
- Kuntsche J, Schuster M, Schneider J. 2019. Engineering design of laminated safety glass considering the shear coupling: a review. Glass Struct Eng. 4:209–228. doi: [10.1007/s40940-019-00097-3](https://doi.org/10.1007/s40940-019-00097-3)
- Kuraray. 2024. Trosifol technical data elastic properties. [accessed 2023 September 6].
- Liang Y, Lancaster F, Izzuddin B. 2016. Effective modelling of structural glass with laminated shell elements. Structures Compos Struct. 156:47–62. doi: [10.1016/j.compstruct.2016.02.077](https://doi.org/10.1016/j.compstruct.2016.02.077)
- LR. 2022. Lloyd's Register, Rules and Regulations for the Classification of Ships, July.
- Magisano D, Leonetti L, Garcea G, Royer-Carfigni G. 2023. A constrained solid-shell model for the geometric nonlinear finite-element analysis of laminates with alternating stiff/soft layers. applications to laminated glass. Int J Solids Struct. 274:112287. doi: [10.1016/j.ijsolstr.2023.112287](https://doi.org/10.1016/j.ijsolstr.2023.112287)
- McMahon S, Scott Norville H, Morse SM. 2018. Experimental investigation of load sharing in insulating glass units. J Archit Eng. 24:04017038. doi: [10.1061/\(ASCE\)AE.1943-5568.0000297](https://doi.org/10.1061/(ASCE)AE.1943-5568.0000297)
- NSIA. n.d. Norwegian Safety Investigation Authority report marine 2023/06: Marine casualty involving the cruise ship 'Viking Polaris' south-east of Cape Horn, 29 November 2022. [accessed 2024 January 10]. <https://www.nsia.no/Marine/Published-reports/2023-06>.
- prEN. 2009. 13474-3 Glass in Building—Determination of the Strength of Glass Panes—Part 3: General Method of Calculation and Determination of Strength of Glass by Testing. European Standard.
- Raikunen J, Avi E, Remes H, Romanoff J, Lillemäe-Avi I, Niemelä A. 2019. Optimisation of passenger ship structures in concept design stage. Ships Offshore Struct. 14:320–334. doi: [10.1080/17445302.2019.1590947](https://doi.org/10.1080/17445302.2019.1590947)
- Respondek Z, Kozłowski M, Wiśniowski M. 2022. Deflections and stresses in rectangular, circular and elliptical insulating glass units. Materials. 15:2427. doi: [10.3390/ma15072427](https://doi.org/10.3390/ma15072427)
- Romanoff J. 2014. Optimization of web-core steel sandwich decks at concept design stage using envelope surface for stress assessment. Eng Struct. 66:1–9. doi: [10.1016/j.engstruct.2014.01.042](https://doi.org/10.1016/j.engstruct.2014.01.042)
- Romanoff J, Remes H, Varsta P, Jelovica J, Klanac A, Niemelä A, Bralic S, Naar H. 2013. Hull-superstructure interaction in optimised passenger ships. Ships Offshore Struct. 8:612–620. doi: [10.1080/17445302.2012.675196](https://doi.org/10.1080/17445302.2012.675196)
- SFS-EN. 2000. 1288-3 Glass in building -- Determination of the bending strength of glass -- Part 3: Test with specimen supported at two points (four point bending).
- SFS-EN. 2015. 12150-1, Glass in building. Thermally toughened soda lime silicate safety glass. Part 1: Definition and description.
- SFS-EN. 2019. 16612 Glass in building. Determination of the lateral load resistance of glass panes by calculation.
- Vallabhan CG, Chou GD. 1986. Interactive nonlinear analysis of insulating glass units. J Struct Eng. 112:1313–1326. doi: [10.1061/\(ASCE\)0733-9445\(1986\)112:6\(1313\)](https://doi.org/10.1061/(ASCE)0733-9445(1986)112:6(1313))
- Wörner JD, Shen X, Sagmeister B. 1993. Determination of load sharing in insulating glass units. J Eng Mech. 119:386–392. doi: [10.1061/\(ASCE\)0733-9399\(1993\)119:2\(386\)](https://doi.org/10.1061/(ASCE)0733-9399(1993)119:2(386))

Appendix. Determination of equivalent laminated thickness

A.1. Bureau veritas

The thickness determination of glass panes in laminated glass according to the Bureau Veritas classification rules is given in Sections 3.3.6 and 3.3.7 (BV 2022) for independent panes and collaborating panes, respectively. That is, the latter includes the shear transfer through the lamination layer. Hence, only that case is of interest and explained here. In this formulation, three different thicknesses are calculated for calculating the response: (1) equivalent deflection thickness, (2) equivalent stress thickness for directly loaded pane, and (3) equivalent stress thickness for indirectly loaded pane. Hence, three separate analyses are needed to obtain the response. If the glass panes are equally thick, then (2) equals (3).

That is, the stresses in both glass panes are identical. Having only one thickness for the deflection implies that the deflection through the thickness of the laminated glass is constant, which is a valid assumption. It should be noted that the presented Bureau Veritas method is identical to that of the ISO 11336-1 standard (ISO 2012, 2023).

The equivalent thickness (t_e) for a laminated glass is chosen as:

$$t_e = \min [t_{1eq,s}, t_{2eq,s}] \quad (A1)$$

where $t_{1eq,s}$ and $t_{2eq,s}$ are the equivalent stress thicknesses for panes one and two, respectively. The stress equivalent thicknesses are calculated as follows:

$$t_{1eq,s} = \sqrt{\frac{t_{eq,d}^3}{t_1 + 2\Gamma t_2}} \quad (A2)$$

$$t_{2eq,s} = \sqrt{\frac{t_{eq,d}^3}{t_2 + 2\Gamma t_1}}$$

where $t_{eq,d}$ is the deflection effective thickness, Γ is the shear transfer coefficient (taking values between 0 and 1 depending on the interlayer material properties), t_1 and t_2 are the pane thicknesses, and t_{s1} and t_{s2} are coefficients. These are given by:

$$t_{eq,d} = \sqrt{[3]t_1^3 + t_2^3 + 12\Gamma l_s} \quad (A3)$$

$$t_{s1} = \frac{hs \times t_1}{t_1 + t_2} \quad (A4)$$

$$t_{s2} = \frac{hs \times t_2}{t_1 + t_2}$$

The coefficients l_s and hs are given by:

$$l_s = t_1 t_{s2}^2 + t_2 t_{s1}^2 \quad (A5)$$

$$hs = 0.5(t_1 + t_2) + t_1. \quad (A6)$$

Finally, the shear transfer coefficient is:

$$\Gamma = \frac{1}{1 + 9.6 \frac{E}{G} \frac{l_s}{hs^2} \frac{t_1}{s^2} \frac{1}{10^6}} \quad (A7)$$

where G is the shear modulus of the interlayer (typically given at 25°C temperature and for 60 s duration load), E is the Young's modulus of the glass panes, and s is the shorter side of the rectangular glass pane.

When the equivalent thickness is calculated according to this procedure, it must be larger than required for a monolithic glass pane:

$$t_e \geq t_r. \quad (A8)$$

The calculation for the required monolithic thickness is shown, for example, in the appendix of Heiskari et al. (2022a).

A.2. Lloyd's register

According to Lloyd's Register rules for laminated glass, the equivalent thickness determination is given in Sections 11.5.2 and 11.5.3 (LR 2022) and is identical to that of Bureau Veritas except for the shear transfer coefficient. While Equation (A8) can be used to calculate the coefficient for any interlayer material properties and rectangular size, Lloyd's Register provides a table for the coefficient for different cases. These are shown in Table A1.

A.3. DNV

The equivalent thickness determination according to DNV classification rules is given in Section 4.2.3 in DNV (2022). The equivalent thickness is calculated as:

$$t_e = \sqrt{\frac{\sum_{i=1}^n t_i^3}{t_{max}}} \quad (A9)$$

where n is the number of layers. This equivalent thickness then must be larger than the required minimum thickness for a monolithic glass pane:

$$t_e \geq t_r. \quad (A10)$$

No specification for the shear transfer is given. However, the thicknesses may be calculated as per ISO 11336-1 standard (i.e. same as Bureau Veritas) if the glass characteristics are determined in a four-point bending test according to EN 1288-3 (SFS-EN 2000) and the interlayer properties are specified by the manufacturer.

A.4. Enhanced effective thickness (Galuppi et al. 2013)

Galuppi et al. have proposed an enhanced effective thickness for laminated glass beams (Galuppi and Royer-Carfigni 2012b), which have been extended to

Table A1. Shear transfer coefficient determination according to Lloyd's Register rules (LR 2022).

Load type	Family 1 (e.g. PVB)	Family 2 (e.g. SGP)
Weather	0.3	0.7
Personnel -- normal	0.1	0.5
Personnel -- crowds	0	0.3

laminated glass panes (Galuppi and Royer-Carfagni 2012a), and its applicability has been demonstrated (Galuppi et al. 2013) also with respect to other methods. Here, an equivalent deflection and stress-effective thicknesses are calculated. The equivalent deflection thickness is:

$$t_{eq,d} = \frac{1}{\left(\frac{\eta}{t_1^3 + t_2^3 + 12l_s} + \frac{1-\eta}{t_1^3 + t_2^3}\right)^{1/3}} \quad (A11)$$

where η is the non-dimensional weight parameter. It is determined as:

$$\eta = \frac{1}{1 + \frac{t}{G} \frac{D_1 + D_2}{D_{tot}} \frac{12D_1D_2}{D_1t_2^3 + D_2t_1^3} \Psi} \quad (A12)$$

where G is the shear modulus of the interlayer, D is the flexural rigidity of the corresponding glass pane, and Ψ is a coefficient depending on the glass pane shape, the load distribution $p(x, y)$ and the boundary conditions. The calculation of Ψ is presented elsewhere (Galuppi et al. 2013), and values are given for multiple different load cases, boundary conditions, and rectangular glass panes sizes. For brevity, only the values of interest in this paper are shown in Figure A1.

The flexural rigidity values are calculated as:

$$\begin{aligned} D_1 &= \frac{Et_1^3}{12(1-\nu^2)} \\ D_2 &= \frac{Et_2^3}{12(1-\nu^2)} \\ D_{tot} &= D_1 + D_2 + 12 \frac{D_1D_2}{D_1t_2^3 + D_2t_1^3} H^2 \end{aligned} \quad (A13)$$

where ν is Poisson's ratio of the glass, E is Young's modulus of the glass, and H is a coefficient given by

$$H = t_i + \frac{t_1 + t_2}{2}. \quad (A14)$$

The quantity l_s is calculated as:

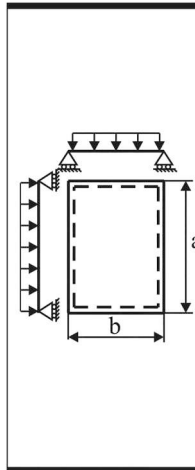
$$l_s = t_1t_{s,2}^2 + t_2t_{s,1}^2 \quad (A15)$$

where $t_{s,1}$ and $t_{s,2}$ are:

$$\begin{aligned} t_{s,1} &= \frac{Ht_1}{t_1 + t_2} \\ t_{s,2} &= \frac{Ht_2}{t_1 + t_2} \end{aligned} \quad (A16)$$

Finally, the equivalent stress-effective thicknesses are:

$$\begin{aligned} t_{1eq,s} &= \frac{1}{\sqrt{\frac{2\eta t_{s,2}}{t_1^3 + t_2^3 + 12l_s} + \frac{t_1}{t_{eq,d}^3}}} \\ t_{2eq,s} &= \frac{1}{\sqrt{\frac{2\eta t_{s,1}}{t_1^3 + t_2^3 + 12l_s} + \frac{t_2}{t_{eq,d}^3}}} \end{aligned} \quad (A17)$$



$\lambda = b/a$	0.1	0.2	0.3	0.4	0.5	0.6	0.7	0.8	0.9	1
500	4018.00	1042.79	486.328	290.422	199.746	150.612	121.070	101.947	88.8653	79.5280
600	2790.28	724.160	337.728	201.682	138.713	104.592	84.0766	70.7962	61.7120	55.2278
800	1569.53	407.340	189.972	113.446	78.0259	58.8328	47.2931	39.8229	34.7130	31.0656
1000	1004.50	260.698	121.582	72.6055	49.9366	37.6530	30.2676	25.4866	22.2163	19.8820
1500	446.445	115.866	54.0364	32.2691	22.1940	16.7347	13.4523	11.3274	9.87392	8.83644
2000	251.125	65.1744	30.3955	18.1514	12.4841	9.41325	7.56690	6.37166	5.55408	4.97050
2500	160.720	41.7116	19.4531	11.6169	7.98985	6.02448	4.84281	4.07786	3.55461	3.18112
3000	111.611	28.9664	13.5091	8.06728	5.54851	4.18367	3.36307	2.83185	2.46848	2.20911
3500	82.0001	21.2814	9.92506	5.92698	4.07645	3.07372	2.47082	2.08054	1.81358	1.62302
4000	62.7813	16.2936	7.59887	4.53785	3.12104	2.35331	1.89172	1.59291	1.38852	1.24262
4500	49.6050	12.8740	6.00405	3.58546	2.46600	1.85941	1.49470	1.25860	1.09710	0.98183
5000	40.1800	10.4279	4.86328	2.90422	1.99746	1.50612	1.21070	1.01947	0.88865	0.79528
5500	33.2066	8.61810	4.01924	2.40018	1.65080	1.24473	1.00058	0.84253	0.73442	0.65726
6000	27.9028	7.24160	3.37728	2.01682	1.38713	1.04592	0.84077	0.70796	0.61712	0.55228

Figure A1. Values of coefficient $\Psi \times 10^{-6} \text{ mm}^2$ for simply supported shape (Galuppi et al. 2014).